KTH ROYAL INSTITUTE
OF TECHNOLOGY

Doctoral Thesis in Physics

Optically poled fibers for electro-optic applications

JOÃO MANOEL BARBOSA PEREIRA

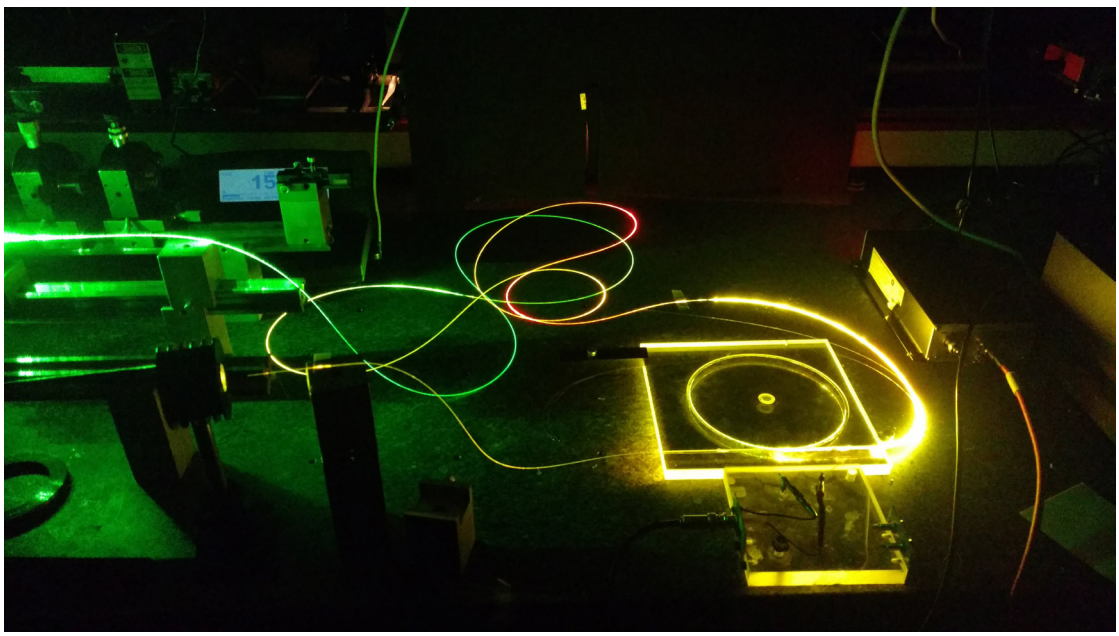

Stockholm, Sweden 2022

Optically poled fibers for electro-optic applications

JOÃO MANOEL BARBOSA PEREIRA

Academic Dissertation which, with due permission of the KTH Royal Institute of Technology, is submitted for public defence for the Degree of Doctor of Philosophy on Wednesday the 15th June 2022, at 10:00 a.m. in FD5, Roslagstullsbacken 21, Stockholm

Doctoral Thesis in Physics
KTH Royal Institute of Technology
Stockholm, Sweden 2022

ISBN 978-91-8040-288-0
TRITA-SCI-FOU 2022:33

Printed by: Universitetsservice US-AB, Sweden 2022

Abstract

The work presented in this thesis shows the development of optically poled devices for use in electro-optic experiments. In the form of papers published, it describes three optical poling methods: green light poling (**Paper I**), poling with a UV lamp (**Paper II**), and corona discharge poling (**Paper V**). Applications using the poled components are studied in distributed sensing by exploring Rayleigh scattering in poled fibers (**Paper III**), intermodal interference in poled fibers (**Paper IV**), and FBG inscribed in poled fibers for voltage sensing (**Paper VI**).

In thermal poling, heat increases the mobility of added ions to the fiber. An external electric field displaces the charges creating a depletion region close to the anode, where the fiber core is usually positioned. The proximity of the metal electrode to the core can cause optical losses, making electro-optic applications less efficient. The need for additional dopant in the preform can make the production of these devices expensive.

Optical poling explores the presence of Ge E' centers in the fiber core to release charges after light excitation. These centers are already present in any fiber with Ge in the core. This enables the development of a fiber for optical poling very similar to a standard telecom fiber, making it cheaper and easy to integrate with standard components. Optical poling does not rely on the formation of a depleted region in the cladding, and the core can be positioned far from the metal electrodes. This advantage allows low-loss electro-optic components to be fabricated.

Optical poling is usually thought to have lower induced effects when compared with thermal poling. In this work, experiments with optical poling were made to study the possibility of increasing the induced second-order nonlinearities to a level comparable with thermal poling.

The fabricated poled fibers were used to investigate their potential use in fiber sensing. The emphasis was to explore new technologies such as CP-ϕOTDR, few-mode fiber sensing, which gained attention in the latest years, and FBGs, which is a mature technology.

The results presented in the **Papers I-VI** show the advances and potential applications explored.

Keywords: Poling, twin-hole fiber, fiber electrodes, optical poling, green light poling, uv poling, corona poling, few-mode fibers, few-mode sensing, FBG sensors, FBG voltage sensors, intermodal interference, electric field sensing.

Sammanfattning

Denna avhandling behandlar optiskt polade fibrer och deras användning i elektro-optiska experiment. Tre olika polningsmetoder har utvecklats och utvärderats; polning med grönt ljus, (**artikel I**), polning med hjälp av en UV lampa (**artikel II**) och Coronaurladdningspolning (**artikel III**). De polade fibrerna utvärderades som komponenter i olika distribuerade sensorexperiment. I **artikel II** utnyttjades Rayleighspridning i fibrerna, i **artikel IV** utnyttjades intermodal interferens i de polade fibrerna och i **artikel VI** användes fiber-Braggitter (FBG) i de polade fibrerna för spänningsmätning.

Vid termisk polning ökar man jonmobiliteten när fibern värms upp. Med ett pålagt elektriskt fält, mellan anoden inne i fibern och katoden utanför, separeras positiva och negativa joner och ett utarmningsområde skapas vid anoden. Efter att jonerna migrerat och temperaturen sänkts fryser jonerna inne på sin nya plats och ett motriktat fält uppstår när det pålagda slås ifrån. Eftersom kärnan är positionerad precis intill anoden hamnar det elektriska fältet över densamma, vilket bryter symmetrin och ger fibern en artificiell inducerad ickelinjäritet. Ett problem kan dock uppstå om avståndet är för kort mellan metallelektroden (anoden) och kärnan, varvid man får betydande utbredningsförluster för ljuset, och i sin tur begränsningar för dess användning i tillämpningen.

Optisk polning utnyttjar närvaron av Ge E' center i fiberkärnan för att frigöra laddningar vid ljusexcitation. Germanium, och därmed Ge E' center, finns som en naturlig dopning i kärnan i standard telekommunikationsfibrer. De väletablerade tillverkningsmetoderna för standardfiber kan alltså användas för att framställa fibrer för polning. Fibrerna blir därmed relativt billiga och de kan lätt integreras med telekommunikationskomponenter.

Optisk polning kräver inget utarmningsområde i manteln, och kärnan kan därmed placeras längre ifrån anoden. Detta gör att man får elektro-optiska komponenter med låga utbredningsförluster. Tidigare var hypotesen att optisk polning gav lägre inducerad ickelinjäritet än termisk polning, och att metoden därmed skulle vara mindre användbar. I detta arbete har vi undersökt möjligheten att skapa en inducerad ickelinjäritet jämförbar med den som åstadkoms vid termisk polning.

De polade fibrerna vi tillverkade utvärderades i flera olika nya fibersensorkoncept. Dessa var CP-ϕOTDR, få-mods fibersensorer, och polade fibergittersensorer. Resultaten presenteras i de sex artiklarna och visar på de betydande framsteg vi nått med fiberpolning och potentialen i de testade tillämpningarna.

Preface

The research presented in this thesis was carried out in the Fiber Optics department at RISE, the Research Institutes of Sweden. The European Commission partially funded this work with the FINESSE project, and the remaining funding was made possible with financial support from prof. Fredrik Laurell from the Laser Physics group at KTH.

The thesis has a brief introduction of the work, a basic theoretical background, the methodology used in the experiments, a summary of the papers published, the conclusion, and the reprints of the publications.

List of Papers

I ***Optical creation and erasure of the linear electrooptical effect in silica fiber***
A. R. Camara,**J. M. B. Pereira**, O. Tarasenko, W. Margulis, and I. C. S. Carvalho
Optics Express **23** (14), 18060-18069, (2015).

II ***Linear electro-optical effect in silica fibers poled with ultraviolet lamp***
J. M. B. Pereira, A. R. Camara, F. Laurell, O. Tarasenko, and W. Margulis
Optics Express **22** (10), 14893-14902, (2019).

III ***Towards Distributed Measurements of Electric Fields Using Optical Fibers: Proposal and Proof-Of-Concept Experiment***
R. Magalhães, **J. M. B. Pereira**, O. Tarasenko, S. Martin-Lopez, M. González-Herráez, W. Margulis and H. F. Martins
Sensors **20** (16), 4461, (2020).

IV ***Electrooptic control of the modal distribution in a silicate fiber***
J. M. B. Pereira, Lars G, K. Rootwitt, G. Town, F. Laurell, and W. Margulis
Optics Express **30** (8), 12474-12483, (2022).

V ***Optical poling by means of electrical corona discharge***
J. M. B. Pereira, O. Tarasenko, Asa Claesson, F. Laurell, and W. Margulis
Optics Express **Accepted**, (2022).

VI ***Voltage sensing using poled fibers and FBG***
J. M. B. Pereira, D. Sartiano, J. Hérvas, D. Barrera, J. Madrigal, S. Sales, F. Laurell, O. Tarasenko, and W. Margulis
Manuscript, (2022).

Description of author contributions

I I worked with the electronic arrangement to generate high-speed pulses for probing the electro-optic fibers. I also helped with the Nd:YAG laser operation.

II I helped with the experiment design, fabricated the fiber components, built the UV lamp poling setup, did the poling experiments with the assistance of my supervisors Walter Margulis and Fredrik Laurell, characterized the fibers for the induced effect, and contributed to the writing of the manuscript.

III I fabricated one fiber component used in the experiments, assisted with the experimental setup, and contributed to the manuscript's writing.

IV I participated in the experiment design with my supervisors and co-authors from DTU, fabricated all the components used in the experiments, built the experimental setup with the assistance of my supervisor Walter Margulis, did the experiments, and helped write the manuscript.

V I participated in the experiment design with my supervisor Walter Margulis, fabricated all the components used in the experiments, built the experimental setup, did the experiments with the assistance of my supervisors, Walter Margulis and Fredrik Laurell, and contributed to the manuscript's writing.

VI I helped with the experiment design, fabricated the components with the help of my supervisor Walter Margulis and co-authors from Universitat Politècnica de València, built the experimental setup, did the experiments, and helped write the manuscript.

Author's publications not included in this thesis

I ***Microsecond switching of plasmonic nanorods in an all-fiber optofluidic component***
S. Etcheverry, L. F. Araujo, G. K. B. da Costa, **J. M. B. Pereira**, Alexandre R. Camara, Jawad Naciri, Banahalli R. Ratna, Iván Hernández-Romano, Christiano J. S. de Matos, Isabel C. S. Carvalho, Walter Margulis, and Jake Fontana
Optica **4**, 864-870, (2017).

II ***Hermetic Carbon Coatings for Electro-Thermal All-Fiber Phase Modulators***
A. Garcia-Ruiz, H. F. Martins, R. Magalhaes, **J. M. B. Pereira**, O. Tarasenko, L. Norin, W. Margulis, S. Martin-Lopez, M. Gonzales-Herraez
Journal of Lightwave Technology **37**, 4567-4572, (2019).

III ***Fiber-based distributed bolometry***
R. Magalhães, A. Garcia-Ruiz, H. F. Martins, **J. M. B. Pereira**, W. Margulis, S. Martin-Lopez, and M. Gonzalez-Herraez
Optics Express **27**, 4317-4328, (2019).

IV ***Twin-core fiber sensor integrated in laser cavity***
J. Amorebieta, **J. M. B. Pereira**, G. Durana, C. Franciscangelis, A. Ortega-Gomes, J. Zubia, J. Villatoro, and W. Margulis
Scientific Reports **submitted**, (2022).

V ***Fabry-Perot cavity optimization for absolute strain sensing using Finite Element analysis***
J. M. B. Pereira, P. M. P. Gouvea, A. M. B. Braga, I. C. S. Carvalho, and A. C. Bruno
Optics Express submitted, (2022).

Conference papers

I ***Pockels fibers by optical poling***
I. C. S. Carvalho, O. Tarasenko, A. R. Camara, **J. M. B. Pereira**, and Walter Margulis
WSOF 2015, Hong Kong (2015).

II ***In-fiber optofluidic alignment of Au-nanorods***
L. F. Araujo, S. Etcheverry, **J. M. B. Pereira**, W. Margulis, J. Fontana, and I. C. Carvalho
WSOF 2017, Limassol (2017).

III ***All fiber based micro-flow cytometer by combining optical fiber with inertial focusing***
L. F. Araujo, S. Etcheverry, G. K. Costa, **J. M. B. Pereira**, A. R. Camara, C. J. De Mator, W. Margulis, J. Fontana, and I. C. Carvalho
LAOP 2016, Medellin (2016).

IV ***Electrical field measurements with poled optical fibers***
J. M. B. Pereira, A. R. Camara, I. C. S. Carvalho, F. Laurell, O. Tarasenko, and W. Margulis
Photonics Sweden, (2017).

V ***Distributed Detection of Optical Radiation using Chirped-Pulse Phase-Sensitive Optical Time Domain Reflectometry***
R. Magalhães, A. Garcia-Ruiz, H. F. Martins, **J. Pereira**, W. Margulis, S. Martin-Lopez, and M. González-Herráez
26th International Conference on Optical Fiber Sensors, (2018).

VI ***Hermetic All-Fiber Phase Modulators Using Joule Heating in Carbon-Coated Fibers***
A. Garcia-Ruiz, H. F. Martins, R. Magalhães, **J. M. B. Pereira**, O. Tarasenko, L. Norin, W. Margulis, S. Martin-Lopez, and M. Gonzalez-Herraez
in 26th International Conference on Optical Fiber Sensors, (2018).

VII ***Distributed detection of quadratic Kerr effect in silica fibers using chirped-pulse ϕOTDR***

R. Magalhães, **J. M. B. Pereira**, A. Garcia-Ruiz, W. Margulis, S. Martin-Lopez, M.l Gonzalez-Herraez, and H. F. Martins
Seventh European Workshop on Optical Fibre Sensors, (2019).

VIII ***High-voltage fiber sensor based on fiber Bragg grating in poled fiber***
J. M. B. Pereira, J. Hervás, D. Barrera, J. Madrigal, S. Sales, F. Laurell, O. Tarasenko, and W. Margulis
Photonics Sweden, (2019).

IX ***High-voltage fiber sensor based on fiber Bragg grating in poled fiber***
J. M. B. Pereira, J. Hervás, D. Barrera, J. Madrigal, S. Sales, F. Laurell, O. Tarasenko, and W. Margulis
Seventh European Workshop on Optical Fibre Sensors, (2019).

X ***Poling Optical Fibers with UV Lamp***
J. M. B. Pereira, A. R. Camara, F. Laurell, O. Tarasenko, and W. Margulis
Conference on Lasers and Electro-Optics - CLEO, (2019).

XI ***High-voltage Sensor Based on Fiber Bragg Grating in Fibers with Electrodes***
J. M. B. Pereira, D. Sartiano, J. Hervas, D. Barrera, J. Madrigal, S. Sales, F. Laurell, O. Tarasenko, and W. Margulis
Conference on Lasers and Electro-Optics - CLEO, (2020).

XII ***Novel Long Period Gratings in Channeled Optical Fibers***
A. Srivastava, F. Esposito, **J. M. B. Pereira**, S. Campopiano and A. Iadicicco
2020 Italian Conference on Optics and Photonics (ICOP), (2020).

XIII ***Fabrication and characterization of arc-induced long period gratings in optical fibers with micro-channels***
A. Srivastava, F. Esposito, **J. M. B. Pereira**, S. Campopiano and A. Iadicicco
IEEE SENSORS, 2020.

XIV ***Poling Optical Fibers with Electrical Corona Discharge***
J. M. B. Pereira, Å. Claesson, F. Laurell, O. Tarasenko and W. Margulis
Conference on Lasers and Electro-Optics Europe & European Quantum Electronics Conference (CLEO/Europe-EQEC), (2021).

XV ***Electrooptic control of the modal distribution in a silicate fiber***
J. M. B. Pereira, Lars G, K. Rootwitt, F. Laurell, and W. Margulis
Conference on Lasers and Electro-Optics - CLEO, (2022).

Acknowledgement

I would like to thank my supervisor Walter Margulis for the trust and for giving me the opportunity of starting this Ph.D. program. From him, I learned everything I know (or I think I know) about fibers and poling. He also helped me by giving me different ideas and solutions for problems I had in the lab without judging my slow thinking. From Walter, I met my supervisor at KTH, Fredrik Laurell, who gave me all the support to continue this work. I also need to thank Fredrik for the funding in my last year. Fredrik was also an essential key in my learning process.

I thank my wife, Carina Braghim Raimundo, for all the support and understanding. Without her, I wouldn't be capable of finishing this work.

I also thank all my family in Brazil.

At RISE, I thank all my colleagues and friends: Carola, Carolina, Kenny, Johan, and Magnus. In particular, I thank Åsa Claesson for the opportunity to work there during my Ph.D. and Erik Zetterlund for hiring me later. I also thank Leif Kjellberg for his assistance and Oleksandr Tarasenko for sharing with me his knowledge; thank you, Sasha. I also thank students, post-docs, and friends that have already left: Frans, Kiana, Harish, Helen, Sanghamitra, and Sebastian.

I thank Michael Folkine for the opportunities and support.

I thank the funding from the FINESSE project. The project made it possible for me to participate in a training network program. I could make many friends, learn, and work in different countries with the help of this project. In particular, I thank Kenny Hey Tow for idealizing this project and Salvador Sales for hosting me at Universitat Politècnica de València for a secondment.

In Sweden, I met only friends. I'm really grateful for being here and that I can work and study freely even without knowing Swedish (I promise I'll practice more Swedish now).

I would like to give special thanks to all my colleagues from my former work at PUC-Rio in Brazil, particularly Isabel Cristina Carvalho and Antonio Carlos Oliveira Bruno. I'll never forget that I was called a scientist by a scientist here.

I thank all the friends I made at KTH, RISE, UPV, and FINESSE ITN. It would be impossible to name all of you.

Acronyms

List of commonly used acronyms:

EDFA	Erbium-Doped Fiber Amplifier
E-FISH	Electric Field Induced Second Harmonic Generation
FBG	Fiber Bragg Grating
FWHM	Full Width Half Maximum
FWM	Four-Wave Mixing
LP	Linearly Polarized
MPA	Multiphoton Absorption
MZI	Mach-Zehnder Interferometer
OFDR	Optical Frequency Domain Reflectometry
OTDR	Optical Time Domain Reflectometry
QPM	Quasi-Phase Matching
SBS	Stimulated Brillouin Scattering
SHG	Second Harmonic Generation
SPM	Self-Phase Modulation
SRS	Stimulated Raman Scattering
STF	Standard Telecom Fiber

Contents

Chapter 1

Introduction

Optical fibers have their primary use in data communication, and are used mainly as passive devices. Over the years, many different techniques were developed to create active photonic devices using fibers. Nowadays, doped fibers with Erbium, Ytterbium, or Neodymium can make active devices such as fiber amplifiers and fiber lasers.

Sensing with fibers is also possible, and Bragg gratings inscribed in fibers (FBGs) are the most used. It is a mature technology usually for measuring strain and temperature. Sensing with fibers can also be distributed, employing techniques such as Optical Time Domain Reflectometry (OTDR) or Optical Frequency Domain Reflectometry (OFDR), achieving a spatial resolution of millimeters and sensitivity of mili-Kelvin or sub-nano strain.

Optical fibers are fabricated using silica glass, which is a centrosymmetric material. Second-order nonlinear effects in a centrosymmetric material are very weak, limiting nonlinear applications such as Second Harmonic Generation (SHG) and electro-optics.

The response to the electric field can be enhanced using poling, a method created to induce an effective second-order susceptibility $\chi^{(2)}_{eff}$ in silicate glasses. This method was first observed in silica glasses by Myers et al. [1] in 1991 and in fibers by Kazansky et al. [2] and Brueck [3] in 1994. Poling records an internal electric field inside the media, creating an electret. In poling, charges are released in the media using an external excitation such as heat or light. The free charges are displaced using an external electric field. The chargers are frozen when the excitation is removed, creating a permanent electric field inside the media.

A poled fiber device is usually made using microstructured fibers with holes from where internal electrodes are added. The fabricated devices can be used for many applications, such as light modulators, light switches, and directional couplers.

Thermal poling is generally the method used for poling fibers, and doped fibers (usually Na^+) are needed to create the free charges after heat excitation.

Optical poling is another poling method that generates free charges in the core using illumination. More discussions of both poling techniques will be made in Chapter 2.

This thesis presents a work with poled fiber components from the design, fabrication, characterization, and possible applications. It shows potential applications for electric field sensing in included papers. The focus is on creating low-loss components with the optical poling method and using them for electro-optic experiments.

1.1 Motivation of the present work

Periodically poled fibers are useful for wavelength conversion in SHG experiments. In this case, the internal electrodes are not used after poling, and are usually removed before application. The metal closer to the core induces optical losses. In electro-optic applications, the internal electrodes are needed to control the refractive index. The electrodes proximity to the core and their long lengths can cause optical losses, making these components undesirable in some applications such as fiber ring lasers or quantum optics applications.

In thermal poling, the core must be close to one electrode, where the depletion region is formed, and the induced nonlinearity is higher. Besides, the poling process needs to be optimized to guarantee that the region where a high electric field is recorded overlaps the core and the propagating wave. In contrast, in optical poling the highest recorded nonlinearity takes place automatically in the core, where the photocarriers are created. The losses can be low, very close to the loss in a standard telecommunication fiber, the disadvantage being the lower nonlinearity induced. While $\chi^{(2)}_{eff}$ of 0.27 pm/V [4] is easily obtained in thermal poling, for optical poling, this number is typically one order of magnitude lower.

Thermal poling has many well-studied parameters to optimize its effects, such as the dopant, the mobility of ions in the glass, the poling temperature, the poling time, and the electrode configuration. It is shown that unconventional electrodes configuration can enhance the induced nonlinearities [5–8].

Optical poling in fibers still does not have a detailed study of its stability, optical power needed for charge generation, different electrode configurations, and many other parameters. A better understanding of the process can unleash potential uses of the technology.

A better description of the differences between optical poling and thermal poling will be given in Chapter 2.

This thesis explores new techniques of optical poling to decrease the gap to a thermally poled fiber, making possible low-loss fiber components based on poled silica. The thesis also explores sensing methods using poled fibers to find new applications.

1.2 Outline of this thesis

In chapter 1 a brief description of optical fibers and poling is given. It also shows the motivation of the work and possible applications of poled fiber components.

In chapter 2 a technical background of electro-optic fiber devices is presented with a basic theoretical explanation.

Chapter 3 shows the design of the fiber components, fabrication, characterization, and the basis for the experiments carried out in the publications included in the thesis.

Chapter 4 presents a summary of the publications included in the thesis highlighting the importance of each paper.

Finally, in chapter 5 are the conclusions that summarize the contributions of this work and plans to improve the experiments discussed in the thesis.

In the appendix is supplemental material for the thesis.

Chapter 2

Background

This chapter gives an introductory background in optical fiber, nonlinear effects, electro-optics, optical fiber sensing, and poling.

2.1 Optical fibers

An optical fiber is a dielectric waveguide in a cylindrical shape based on the principle of total internal reflection of light. It is made with two fundamental structures: the core and the cladding. Additional structures, such as the coating and the jacket, are added to protect the fiber and guarantee that it can be used in different environments. A schematic representation of the structures of a typical optical fiber is given in the figure 2.1a. The core has a slightly higher refractive index than the cladding and ensures the total reflection, keeping the light in the core. In Figure 2.1b it is shown a representation of the refractive index profile for a step-index fiber where r_{core} and r_{clad} are the radius of the core and the cladding respectively. Another index profile commonly found is graded-index [9].

The core diameter defines the number of spatial modes guided in the optical fiber. If the core is small enough for a particular wavelength, only a single mode is permitted, and the fiber is said to be single-mode. Larger core diameters permit more modes to be guided, and the fiber is said to be multimode. Each mode has an intrinsic propagation constant and group velocity. The number of modes guided in an optical fiber can be determined using the waveguide parameter, the *V-number* [9], expressed as:

$$V = \frac{\pi d_{core} N}{\lambda} \tag{2.1}$$

where d_{core} is the core diameter, λ is the wavelength guided in the fiber, and N is the numerical aperture of the optical fiber, defined by [9]:

$$N = \sqrt{n_{core}^2 - n_{clad}^2} \tag{2.2}$$

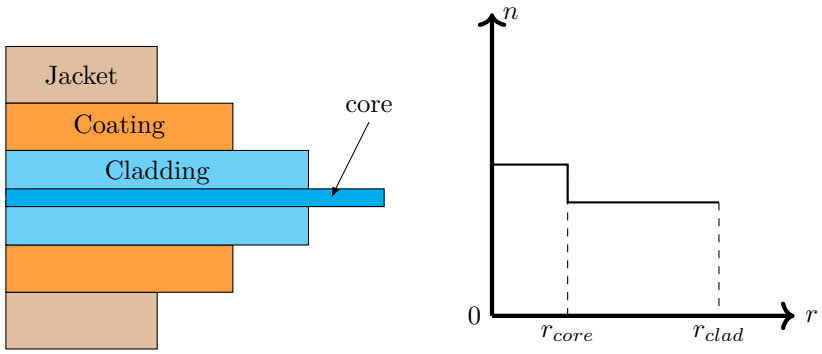

Figure 2.1: a) Typical structure of an optical fiber used in telecommunication. The core typically has 8 μm*, the cladding* 125 μm*, the coating* 250 μm*, and the jacket* $>$ 400 μm*. b) Refractive index profile in a step-index optical fiber.* r_{core} *and* r_{clad} *are the radius of the core and the cladding, respectively.*

where n_{core}, is the refractive index of the core, and n_{clad} is the refractive index of the cladding. If $V < 2.405$ in a step-index fiber, only one Linearly Polarized (LP) mode is supported, the fundamental LP_{01} and the fiber is single-mode. Higher *V-number* allows multimode operation. In a multimode fiber, the first six LP_x polarization degenerated modes are represented in Figure 2.2. Multimode fibers are not frequently used for communication over long distances due to modal dispersion, and single-mode fibers are preferred for this end [9].

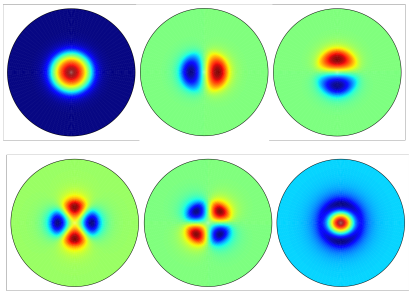

Figure 2.2: The first six polarization degenerated modes found in optical fibers: LP_{01}*,* LP_{11a}*.* LP_{11b}*,* LP_{21a}*,* LP_{21b}*,* LP_{22}*. From* ***Paper IV****.*

2.2 Nonlinearities in optical fibers

Nonlinearities in fibers are a disadvantage in optical communications because they limit the maximum light intensity, decreasing the communication range [10]. Nev-

ertheless, nonlinearities are useful for pulse compression, fiber amplifiers, wavelength conversion, supercontinuum generation, fiber lasers, and electro-optics.

Nonlinear effects are caused by the interaction of the light electric field with the medium [11]. There are two different types of nonlinearities: generated from scattering such as Stimulated Brillouin Scattering (SBS) and Stimulated Raman Scattering (SRS), and from induced index changes that result in Self-Phase Modulation (SPM), parametric processes such as Four-Wave Mixing (FWM) and Second Harmonic Generation (SHG) [10, 12].

In a nonlinear media, the polarization of the light P is affected by the electric field E with the expression [12]:

$$P(E) = \epsilon_0 \left(\chi E + \chi^{(2)} E^2 + \chi^{(3)} E^3 \right) \tag{2.3}$$

where ϵ_0 is the permittivity in free space, χ is the linear susceptibility, $\chi^{(2)}$ and $\chi^{(3)}$ are the second-order and third-order nonlinear coefficients. Higher-order terms are often neglected [12]. A linear dependence with the field characterizes a linear media, and only the first term is used: $P(E) = \epsilon_0 \chi E$. The linear refractive index n is associated with χ and the relative permittivity of the material ϵ with the equation:

$$n^2 = \epsilon / \epsilon_0 = 1 + \chi \tag{2.4}$$

Due to the symmetry of the silica, nonlinearities in an optical fiber are limited to third-order nonlinear effects, and it is a weak effect. However, second-order effects can be induced if a high electric field is applied to the media resulting in effects such as Electric Field Induced Second Harmonic Generation (E-FISH) [13], or via poling [1], which freezes an electric field in the media [14]. The added field generates a cascaded $\chi^{(3)}$ parametric process [10]. Poling can be used to create parametric optical components for Second Harmonic Generation [15, 16] and active electro-optic components [17] such as optical modulators and optical switches. More information about poling is in the following sections of this thesis.

The mathematical description for the electric field interaction with a nonlinear media is described in greater detail in the Appendix A.

2.2.1 Standard Telecom Fibers (STF)

Standard Telecommunication Fibers (STF), also known as SMF-28 [18], are developed to optimize data communication over long distances, ensuring high-speed transmission in a low loss-media. The advantage of an STF fiber over electrical wires often mentioned is the capability to create lightweight waveguides with cheap and abundant material (silica). Optical fibers are also immune to electromagnetic interference. The STF is optimized to guide light in the *c-band*[1] region

[1]The conventional band, ranging from 1530 nm to 1565 nm.

of the optical spectrum. The core has 8 μm, and the cladding has a 125 μm diameter. The refractive index of the core is 1.45 at 1550 nm, and it is higher than the index of the cladding by $\Delta n \approx 0.005$ due to germanium doping of the core. STF fibers are single-mode at 1550 nm ($V = 1.95$).

2.2.2 Optical fiber sensing

Apart from the primary use of optical fibers in telecommunication, fibers can also be used for sensing [19, 20]. Different techniques are explored, and in most cases, sensing is linked to variations of the refractive index in the fiber due to an external perturbation. The perturbation in the refractive index causes a phase change in the light and can be detected and quantified using an interferometer [19] such as Mach-Zehnder, Michelson, or Sagnac.

Other sensing methods with fibers explore the external index variation, such as in fiber-based Fabry-Perot interferometers [21, 22] or changes in the propagating field caused by plasmon resonance [23].

Perturbation in the refractive index in the fiber core is usually due to strain, via the stress-optic effect, or temperature, via the thermal-optic effect. Other physical parameters are commonly measured by converting the physical parameter to strain. The index can also be changed with the electric field, the electro-optic effect [12], a subject of this thesis.

Next, some relevant sensing methods are presented for the thesis.

Fiber Bragg Gratings

Fiber Bragg Gratings (FBGs) are probably the most used technique in fiber sensing. FBGs are optical fibers with a periodic structure in the core. The simplest case is an uniform inscribed grating, as shown in Figure 2.3a, formed by an alternating refractive index (Figure 2.3b) along the fiber. It reflects a specific light wavelength (the Bragg wavelength, λ_B) and transmits the others (Figure 2.3c).

FBGs are largely applied for sensing because the reflected light, affected by the refractive index changes, is easy to measure with reasonable accuracy. A typical FWHM (Full width at half maximum) bandwidth of a reflected wavelength is around 200 pm. FBG sensing is a mature technology and finds applications in many different fields. The Bragg wavelength is defined by [24]:

$$\lambda_B = 2n_e\Lambda \tag{2.5}$$

where n_e is the mean effective refractive index at the grating location. The sensitivity of the FBG to strain can be calculated using [24]:

$$\Delta\lambda_B = \lambda_B(1 - p_e)\varepsilon \tag{2.6}$$

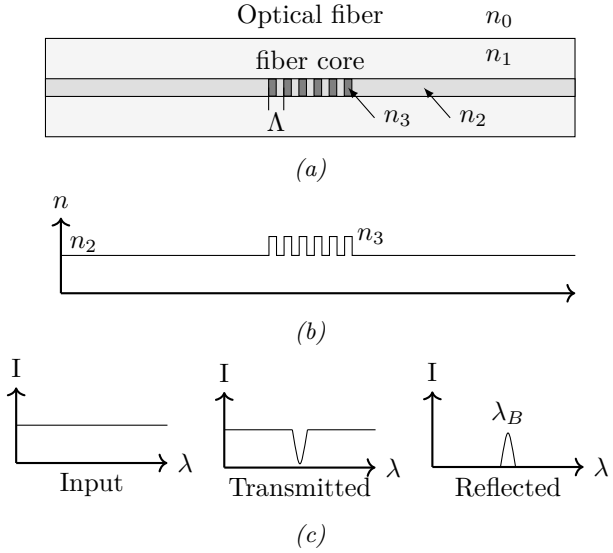

Figure 2.3: The structure of an FBG showing the refractive index periodicity in the core and the optical spectral response. a) n_0 is the refractive index outside the fiber, n_1 is the cladding refractive index, n_2 is the core refractive index, and n_3 is the refractive index of the inscribed periodic structure with period Λ. b) The refractive index along with the core. c) When a broadband light input is launched into the core, the inscribed grating reflects the Bragg wavelength, denoted by λ_B.

where p_e is the effective strain-optic constant and $\varepsilon = \Delta l/l$ is the strain. If the FBG is inscribed in a standard telecom fiber $p_e = 0.22$ and the sensitivity to strain (wavelength shift) is 1.2 pm/$\mu\varepsilon$ at $\lambda_B = 1550\,\text{nm}$.

For temperature sensing, the wavelength shift with a change in temperature ΔT can be calculated with [24]

$$\Delta\lambda_B = \lambda_B(\alpha_\Lambda + \alpha_n)\Delta T \tag{2.7}$$

where α_Λ is the thermal expansion coefficient ($\approx 0.55 \times 10^{-6}\,°\text{C}^{-1}$ for silica) and α_n is the thermo-optic coefficient ($\approx 8.6 \times 10^{-6}\,°\text{C}^{-1}$ for a germanium doped silica). At $\lambda_B = 1550\,\text{nm}$ the sensitivity of an FBG to temperature is 14.8 pm/°C.

Sensing with multimode fibers

Multimode fibers have applications in telecommunication [25], quantum optics [26], image processing, optical switches [27], and sensing [28, 29]. Sensing with a multimode fiber is particularly interesting because each mode can sense perturbations individually [28, 30] since the modes propagates independently [9].

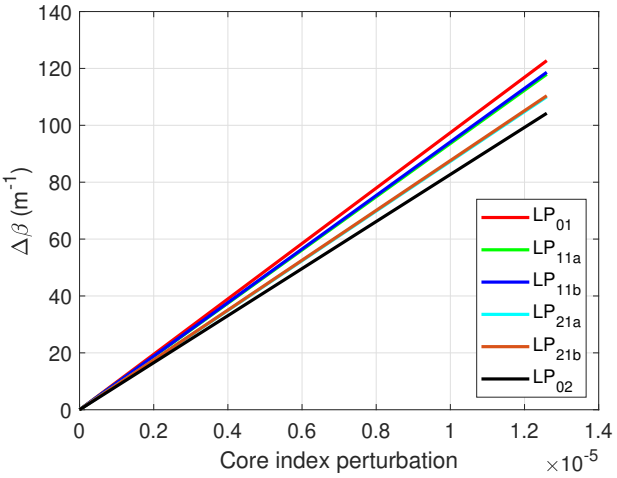

Figure 2.4: Propagation constant changes when a uniform index perturbation is applied over 1 m of fiber, from ***Paper IV****.*

Sensing can also be done with a multimode fiber by exploring the different group velocities of the modes. The phase difference, caused by refractive index changes, leads to intermodal interference [29]. Intermodal interference in fiber with a few-modes is conveniently used for sensing because it works as an interferometer in a single fiber [31] being less susceptible to instabilities. Figure 2.4 shows the effect in the propagation constant β [9] for the first six polarization degenerated modes when a uniform perturbation is applied over 1 m multimode fiber.

Distributed sensing

Distributed sensing using fibers takes advantage of spontaneous light scattering in the glass to quantify an external perturbation. The advantage of such sensors, among others, is the possibility of having a single-ended passive fiber component capable of measuring in real-time external parameters such as temperature and strain over long distances [32].

The light scatting in glass is a statistical process and can be a linear process (Rayleigh) or a nonlinear process (Brillouin and Raman). The generalized scattered spectrum response is illustrated in Figure 2.5.

Rayleigh is an elastic process, and the wavelength of the scattered light remains the same as the light that originated it. It is caused by material-density fluctuations in the media [32]. Brillouin scattering originates from light interaction with acoustic phonons, and Raman originates from molecular vibra-

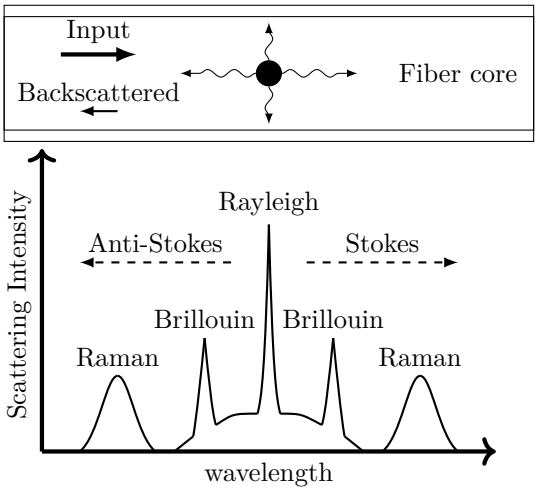

Figure 2.5: The spectrum of spontaneous light scattering processes.

tions [32,33]. An external perturbation in the optical fiber can affect the scattering process in all variants.

Different techniques, such as Optical Time Domain Reflectometry (OTDR) and Optical Frequency Domain Reflectometry (OFDR), are used in distributed sensing. It usually analyses the backscattered light with synchronized detection to localize the point of interest in the fiber.

2.3 Electro-optic effect

The electro-optic effect is the change of the refractive index in a media due to an external electric field. The refractive index dependence with the field can be expressed as a Taylor expansion [12]:

$$n(E) = n_0 + \left(\frac{dn}{dE}\right)\Big|_{E=0} E + \frac{1}{2}\left(\frac{d^2n}{dE^2}\right)\Big|_{E=0} E^2 + \cdots \tag{2.8}$$

The second and third terms are order of magnitude smaller than n, and higher-order terms are frequently neglected. It is common to write equation 2.8 in terms of the nonlinear coefficients $\chi^{(2)}$ and $\chi^{(3)}$. Doing so Equation 2.8 assumes the form:

$$n(E) = n_0 + \frac{\chi^{(2)}}{n_0} E + \frac{3\chi^{(3)}}{2n_0} E^2 \tag{2.9}$$

The second term on the right side of Equation 2.9 responds linear with the field, and it is related to the Pockels effect. The third term responds quadratically to the field, the Kerr effect.

2.3.1 Pockels effect

When the refractive index of the material responds linearly to the electric field, shown in Figure 2.6, it is said that the media is a Pockels medium. From Equation 2.9 the linear term is dominant, and the refractive index changes can be expressed as:

$$n(E) = n_0 + \frac{\chi^{(2)}}{n_0} E \tag{2.10}$$

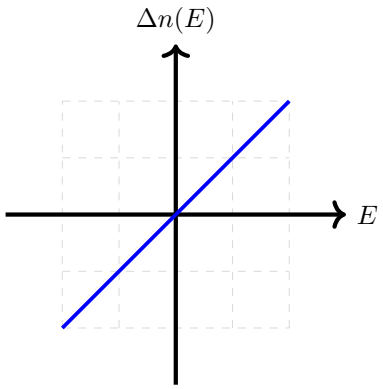

Figure 2.6: Linear response of the refractive index with the electric field: Pockels's effect.

The Pockels effect is restricted to materials without inversion symmetry, such as lithium niobate and other noncentrosymmetric media. Since the electric field is applied in a specific orientation, it is expected to raise birefringence.

A Pockels cell is a wave-plate controlled with voltage. The changes in refractive index due to the applied voltage create phase retardation of the light. Due to the birefringence, a slow and a fast axis is created with the field. The difference in the propagation speed between the two orthogonal polarizations changes the polarization that emerges in the Pockels cell. For example, a linear polarized light incident at 45°with the fast and slow axis would become a circularly polarized light after the cell due to the phase difference in both polarization components [12]. If a polarizer is placed after the emerging circular polarized light, a change in intensity is seen for different voltages biasing the Pockels cell. These components find many applications, such as Q-switching lasers or light modulation. It offers faster responses when compared with acousto-optic or liquid crystal based devices.

Pockels components have significant use in telecommunication to fabricate light intensity modulators. The difference in phase caused by a voltage bias is translated to an intensity variation in an interferometer. An important quantity

evaluated in such components is V_π, the voltage necessary to change the phase of the light by π, causing total extinction of the light. It depends on the component's dimensions, the linear nonlinearity, and the wavelength of the guided light. The linear nonlinearity is often described as the Pockels coefficient r [4, 12]:

$$r = \frac{2\chi^{(2)}}{n_0^4} \tag{2.11}$$

If the electric field in the media is assumed to be $E = V/d$, where V is the voltage applied across two faces of a cell with length L separated by a distance d, as seen in Figure 2.7, V_π is [12]:

$$V_\pi = \frac{d}{L}\frac{\lambda}{rn_0^3} = \frac{d}{L}\frac{\lambda n_0}{2\chi^{(2)}} \tag{2.12}$$

where λ is the optical wavelength. A typical value for V_π in a commercial Pockels cell is 5 kV @ 800 nm [34]. For a lithium niobate intensity modulator used in telecommunication it can be as low as 2 V @ 1550 nm for 1 GHz modulation [35]. As shown in Equation 2.12, V_π is dependent on the dimensions of the Pockels material and the guided wavelength. If the same wavelength and material is used, V_π can decrease from 5 kV to 2 V by simply reducing the separation between electrodes from 1 mm to $\approx 2\mu$m. V_π is also known as *half-wave voltage*.

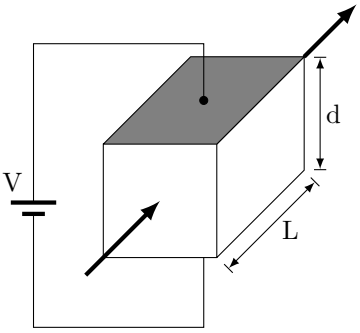

Figure 2.7: A transverse electro-optic modulator with length L and parallel plate electrodes separated by a distance d. The phase of the light (represented with the arrows) is affected by the voltage V applied to the electrodes.

2.3.2 Kerr effect

In a symmetric material, the refractive index changes due to the electric field must be a symmetric function since it is invariant to the polarity of E, as it can be seen in Figure 2.8. In this case, the linear component of Equation 2.9 is zero. Such material is known as a Kerr medium, and the refractive index dependence with the electric field is:

$$n(E) = n_0 + \frac{3\chi^{(3)}}{2n_0}E^2 \tag{2.13}$$

From Figure 2.8 it is clear that the refractive index changes are small around $E = 0$ and gets significance only for high electric fields.

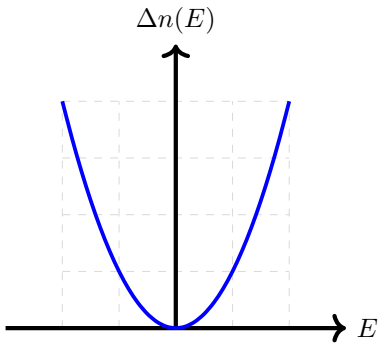

Figure 2.8: Quadratic response of the refractive index with the electric field: Kerr effect.

Examples of a Kerr media are gases, liquids, certain crystals, and amorphous materials such as glass. Since its effect is very weak (compared with the Pockels effect) and the quadratic response makes the correlation between Δn and E (or V) more difficult than the linear dependence, the effect is not very explored in electro-optic devices. Typical values for the third-order nonlinear coefficients in such materials are of the order of 10^{-22} to 10^{-16} $\mathrm{m}^2/\mathrm{V}^2$. In silica glass ($\chi^3 \approx 2 \times 10^{-22}\,\mathrm{m}^2/\mathrm{V}^2$ [36]) a refractive index changes of the order of 10^{-6} is expected when a field of $E = 1 \times 10^8\,\mathrm{V/m}$ (i.e., 10 kV applied to 100 μm separated electrodes) is applied. The optical phase changes caused by this small effect can be measured in long waveguides, such as an optical fiber.

2.4 Poling

Similar to a magnet, where a permanent magnetic field is stored in a magnetic material, an electret is created when an electric field is stored in a dielectric material. Electrets have many applications, where the most famous is the electret microphone.

The permanent field in electrets is created by exposing the dielectric to an intense field while an external excitation is applied, allowing charge displacement. Nadjakov noted that it is possible to induce electric polarization in some materials by exposing them to light with an externally applied electric field [37, 38]. The previously recorded field can be erased when exposed to light without an external field.

If the electret is a transparent material, other interesting effects can be explored when light propagates in it. The process of recording an electric field in a dielectric optical media is called poling.

In an amorphous material, such as glass, the nonlinearity is weak and governed by the third-order nonlinear coefficient $\chi^{(3)}$ since $\chi^{(2)}$ is absent, as seen in section 2.3.2. If Equation 2.13 is used to describe the electro-optic effect in glass and E becomes the sum of externally applied field E_{app} and the recorded field E_{rec}, (i.e. $E = E_{app} + E_{rec}$) Equation 2.13 can be rewritten as:

$$n(E) = n_0 + \frac{3\chi^{(3)}}{2n_0}(E_{app} + E_{rec})^2 \tag{2.14}$$

$$n(E) = n_0 + \frac{3\chi^{(3)}}{2n_0}E_{rec}^2 + \frac{3\chi^{(3)}E_{rec}}{n_0}E_{app} + \frac{3\chi^{(3)}}{2n_0}E_{app}^2 \tag{2.15}$$

the third term on the right side of Equation 2.15 responds linearly to an externally applied field E_{app} and the last term quadratically. The linear term shows a Pockels behavior and can be compared with the linear term in Equation 2.9, while the third term exhibits a Kerr response [39]. Poling in glass can induce a linear response by inducing an effective $\chi^{(2)}_{eff}$ in the material:

$$\chi^{(2)}_{eff} = 3\chi^{(3)}E_{rec} \tag{2.16}$$

The effect of poling a Kerr media can be visualized with the help of Figure 2.9, where the refractive index changes linearly around $E = E_{rec}$ (instead of $E = 0$) for small changes of the externally applied field, E_{app}.

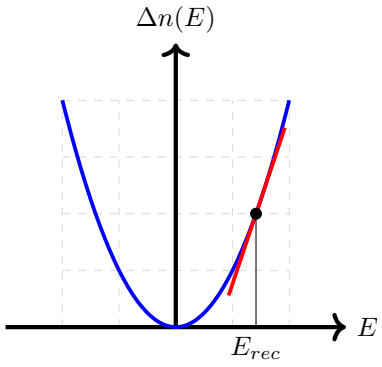

Figure 2.9: Poling has the effect of inducing a linear working regime around $E = E_{rec}$ instead of around $E = 0$ seen in a Kerr media.

Glass poling is usually made by increasing the mobility of the charges in the glass with heat while exposing them to a high electric field. After cooling down the material in the presence of the field, the charge mobility decreases and the charges are now frozen. A method known as thermal poling [1].

The new charge distribution induces nonlinearities that can be explored for optical modulation in an electro-optic device or Second Harmonic Generation (SHG).

As mentioned for electrets, the recorded field of a poled material can be erased if exposed to light [40]. The guided light in the poled device might not exceed the energy necessary to erase the internal field.

Periodic poling, by poling with assisted erasure with UV [40], can increase the SHG generation efficiency by taking advantage of Quasi-Phase Matching (QPM) [13, 41]. QPM can increase the SHG efficiency by periodically changing the relative optical phase of the generated second-harmonic waves [42]. This method prevents the generated wave from interacting destructively with previous second-harmonic waves.

Optical fibers can also be poled, and fiber with internal electrodes is usually used. The first demonstration of a poled optical fiber was made by Kazansky [2] and Brueck [3] independently when D-shaped fibers were poled. Poled fibers have applications in all-fiber optical modulators, optical switches, and electric field sensing, to cite a few.

2.5 Poling optical fibers

2.5.1 Thermal poling

Thermal poling is the most widely used technique to pole fibers. In thermal poling, a doped preform with Na^+ is usually used [43]. The added cations are made mobile using heat and displaced with an external field, giving rise to an internal electric field. The created internal field is frozen when the fiber is cooled down [1].

The poling temperature is usually between 250-290°C [1], and at this temperature, the added ions are mobile and migrate in the glass matrix [43, 44].

During thermal poling, a charge distribution takes place. The process consists of the movement of cations from the anode to the cathode and charge recombination near the electrode. During this process, in the absence of replenishment of chargers from the anode, a depleted region, free of cations, is created [4].

The depletion region is formed close to the anode, where the highest electric field is formed. Ideally, the depleted region is $\approx 10\mu$m thick, and the fiber's core is inside this region.

In thermal poling, many parameters must be monitored during the poling process. The temperature impacts the mobility of the ions, and the poling time influences the formation of the depleted region [45, 46].

The proximity of the core to the metal electrode leads to an optical loss in thermally poled electro-optic components. The optical losses in such devices can be higher than 10 dB/m at 1550 nm [47].

Different dopants can be used in thermal poling, such as Na^+, Li^+, and K^+ [43] and the mobility of the different ions can be used to enhance poling. It was also found that unusual electrodes configuration, such as two anode poling [5], can increase the poling efficiency and the recorded field can be higher than the applied electric field during poling.

2.5.2 Optical Poling

Optical excitation can free charges in a silicate fiber core, forming a frequency doubling grating [48–50]. It was also found that the formed frequency doubled grating can be erased using light [15, 51]. Since UV exposure can create periodic index changes in the core for FBG fabrication, it is expected that UV light can release charges, which are useful for optical poling.

In optical poling, photocarriers are generated in the core when short-wavelength light (e.g., UV, blue or green radiation) excites the Ge-doped silica. In the presence of an applied electric field, the photocarriers (electrons and holes) are displaced, generating an internal field in the core that is frozen when the light excitation is removed. Optical poling can be done at room temperature. Since the internal electric field is in the core, the core position between the electrodes is not relevant. The core can be positioned far enough from the metallic electrode to avoid optical losses. This advantage opens possibilities for low-loss active devices, enabling applications in quantum optics, sensing, and intra-cavity fiber lasers, where the loss can play a critical role.

The creation of free charges in silica due to photoexcitation is related to the presence of Ge E' centers in the core [52]. Germanium doped silica has an absorption band at ≈5.1 eV (≈ 244 nm) [53], which can be accessed by multiphoton absorption (MPA) if the light intensity is high. The probability of MPA increases with the light intensity [54]. The free charges are electrons and holes released by photoexcitation, and they are naturally trapped in the silica matrix [55], where they remain frozen.

It is shown experimentally that the Ge available in the core of a twin-core STF-like fiber is sufficient to record an internal field as high as $\approx 2\times10^8$ V/m [17]. Using an STF-like fiber for optical poling can result in devices that are easily integrated into available optical components. The limiting factor seems to be the electric field applied during poling. It is found that the higher the field established during optical poling, the higher the recorded field and the higher the linear electro-optic effect induced.

To estimate of the number of free charges needed for optical poling, the approximation $Q = CE_{rec}d'$ can be used, where Q is the displaced charge in the core, C is the capacitance, E_{rec} is the recorded field, and d' is the charges separation distance. The capacitance C in 1 m long STF fiber with 8 μm core

and assuming that the charges are displaced by a distance $d = 8 \times 10^{-6}$ m is $C = \epsilon_r \epsilon A/d = 3.8 \times 8.85 \times 10^{-12} \approx 34$ pF. For a recorded field of 1×10^8 V/m the total displaced charge is $Q = 2.72 \times 10^{-8}$ C or 1.7×10^{11} elementary charges needs to be displaced in the core. The concentration of Ge E' centers in a Ge doped silica fiber is $> 1 \times 10^{15}$ centers/cm^3 [56] which shows that the limiting factor of optical poling is the poling field.

In optical poling, it was also found that the recorded field E_{rec} has the opposite polarity than the field applied during poling [57]. This is because the charges are displaced to neutralize the external field, creating an opposite field in the core.

Early experiments with UV poling showed a large induced nonlinearity of $\chi^{(2)} \approx 13$ pm/V [58] in 1995, which motivated much research in the field. The experiment used 193 nm light from a ArF laser illuminating the core while an electric field was applied to the fiber's internal electrodes. Nonetheless, many research groups failed to reproduce the results, and only a fraction of the coefficient was obtained [59]. The difficulty in replicating the results and the low nonlinearity frequently found demotivated further research in optical poling.

Although even with the low nonlinearity induced when compared with thermal poling, optical poling is still an interesting topic of study due to its advantages and possible applications.

The induced nonlinearity obtained by optical poling is still lower than what can be obtained by thermal poling. A typical value obtained is $\chi^{(2)} \approx 0.05$ pm/V.

2.6 Electro-optic amplitude modulation

Due to a voltage bias, the optical phase modulation caused by an electro-optic component can be converted to intensity modulation if the active component is in one arm of an interferometer. A Mach-Zehnder Interferometer (MZI), as seen in Figure 2.10a, is often used for this end.

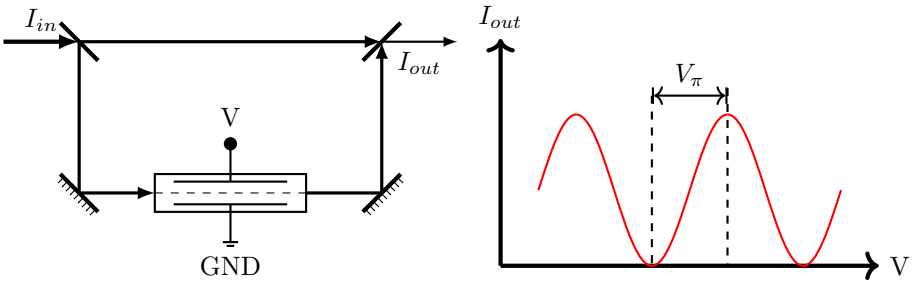

Figure 2.10: A phase modulator built with an active fiber component in one arm of an interferometer can be utilized as an intensity modulator. The voltage applied to the component changes the transmitted light intensity periodically.

The phase changes with index in an interferometer are described with [12]:

$$\phi(E) = \frac{2\pi n(E) l}{\lambda} \tag{2.17}$$

where $n(E)$ is the refractive index changes with an electric field, l is the optical path of the active component, and λ is the probing wavelength. If Equation 2.14 is used for $n(E)$, the phase changes can be rewritten:

$$\phi(E) = \phi_0 + \frac{3\pi l \chi^{(3)}}{n_0 \lambda} \left(E_{app} + E_{rec}\right)^2 \tag{2.18}$$

where

$$\phi_0 = \frac{2\pi l}{\lambda} n_0 \tag{2.19}$$

The imbalance $\Delta\phi(E_{app})$ caused by changes in the applied electric field E_{app} causes changes in the intensity of the transmitted light (I_{out}) in the interferometer [12]:

$$I_{out} = \frac{I_{in}}{2} \left\{1 + cos\left[\Delta\phi(E_{app})\right]\right\} \tag{2.20}$$

Using Equation 2.18 in 2.20 and assuming $E_{app} = V_{app}/d$, the intensities relationship I_{out}/I_{in} can be written as:

$$2\frac{I_{out}}{I_{in}} = 1 + cos\left[\frac{3\pi l \chi^{(3)}}{n_0 \lambda}\left(E_{rec} + \frac{V_{app}}{d}\right)^2 - \phi_0^{'}\right] \tag{2.21}$$

The light intensities (I_{in} and I_{out}) are proportional to voltage measured with a photodetector. $\chi^{(3)}$ and E_{rec} can be obtained if Equation 2.21 is used to fit an interferometric curve obtained by measuring the transmitted light intensities for different V_{app} (similar to the curve in Figure 2.10b).

Various types of interferometers can be built to characterize the electro-optic effect in fibers, giving relatively good accuracy on the V_π (the applied voltage necessary to go from minimum to maximum light intensity, as shown in Figure 2.10b) and the induced $\chi^{(2)}_{eff}$ (obtained with E_{rec} and Equation 2.16). Fiber-based Mach-Zehnder interferometers have the disadvantage of being unstable with temperature fluctuations (requiring active stabilization), making them difficult for unattended applications. Another interferometer often used is the Sagnac, which has the benefit of being insensitive to temperature but requires fast pulses and/or long delay lines inside the Sagnac loop.

Chapter 3

Fabrication and characterization of electro-optic fiber components

This chapter focus on the experimental work of this thesis. It shows details of the fibers used in the experiments and the fabrication of the electro-optic components. It discusses the optical poling procedure and the characterization of the induced electro-optic effect. Characteristics such as optical losses, stability, and polarization dependence are also discussed.

3.1 Optical fiber for optical poling

In electro-optic experiments with fibers, metal inserted into fiber with internal holes can be used as electrodes to which voltage can be applied. In a parallel plate configuration, the electric field between the electrodes is $E = V/d$, where V is the voltage applied, and d is the separation of the electrodes. In optical poling, the higher the electric field, the higher is the induced electro-optic effect [17] implying that fiber for optical poling should have the electrodes as close as possible but far enough to avoid optical losses.

A twin-hole fiber made from an STF fiber can conveniently be used in optical poling experiments. The amount of charges generated in the core is sufficient for saturation of the induced effect [17]. Two holes with $\approx 30\,\mu$m in diameter are large enough to be filled with a thin wire or liquid metal and be still small enough not to compromise the mechanical structure of the fiber. In previous studies with thermal poling, it was found that a metal electrode placed more than $10\,\mu$m from the fiber core is sufficient to provide a low-loss media.

3.2 Twin-hole fiber

The holes of the twin-hole fiber are made by drilling holes into the preform. The geometrical shape of the preform is preserved in the fiber after drawing. The

preform has typically 25 mm in diameter that will become 125 μm after drawing. To create a 30 μm hole in the final fiber 6 mm hole is made in the preform. The fiber is drawn colder than the normal used temperature to avoid the holes from collapsing. The typical drawing speed is between 20 and 30 m/min. Figure 3.1 shows the twin-hole fibers used in the experiments with optical poling.

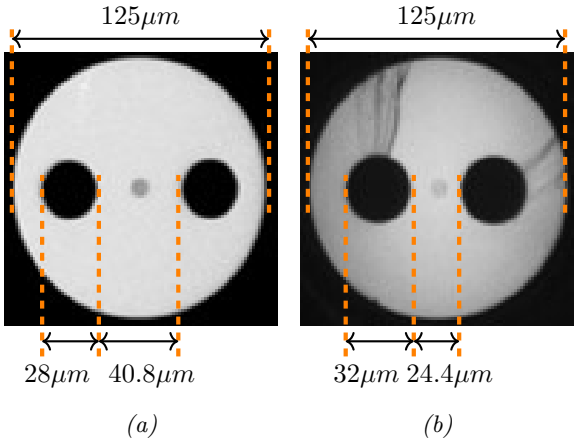

Figure 3.1: Twin-hole fibers are used for optical poling experiments. The fibers are made by drilling holes into an STF preform. a) Fiber with 40.8 μm electrodes separation and 28 μm holes diameter. This fiber is coated with acrylate. b) This fiber has slightly larger holes (32 μm) with 24.4 μm separation; it is polyimide coated.

Electrodes are made by inserting metal into the fiber holes. Thin wires can be used, but the length of the wires inserted is very limited in a manual process, and only a few centimeters can be easily inserted. This method consists of polishing the fiber from the side, accessing the hole, and inserting the wire, usually with the help of tweezers and a microscope. Besides the practical difficulty to insert long wire lengths, the position of a thin wire in the hole is undetermined, and the field applied during and after poling is unknown and varies along the fiber.

Liquid metal pumped into the holes is also used, and it can provide a very uniform electrode since the metal fills the entire volume inside the hole. Meters of electrodes can be made with this method [60]. Liquid metals, such as mercury or gallium, are usually used for thermal poling when second harmonic generation is the objective since it can be easily pumped out after poling.

Metal with a low melting point, such as BiSn, which melts at 137°C, is also used as electrodes. It is pumped in a molten state and is solid at room temperature. A solid electrode enables applications in electro-optic experiments where the contacted electrodes can be easily connected to other devices. It is the method used in the experiments of this thesis. Other alloys are also frequently

used, such as AuSn, which has a higher melting point (280°C).

3.3 Electrode filling

The fibers with internal electrodes used in this work are made by filling the empty holes with BiSn in a molten state. To this end, an oven and a pressure cell are used, Figure 3.2. The pressure cell has an inner container for the BiSn metal, and it is heated to 160°C inside the oven. The fiber section to be filled is inserted into the oven. The fiber tip is inserted into the pressure cell and immersed in the molten metal.

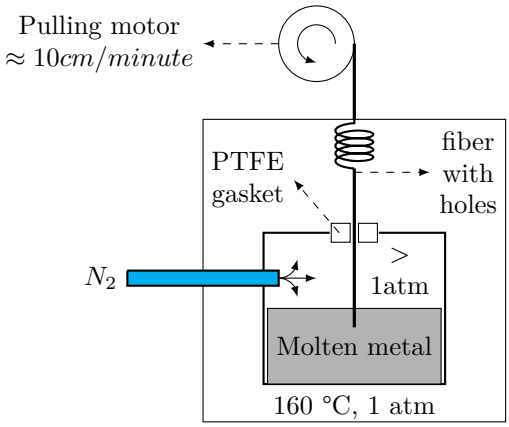

Figure 3.2: Schematic drawing of the equipment used for filling the fiber's holes with metal. Pressure from a N_2 bottle is used to pump molten BiSn alloy. A pulling motor slowly removes the fiber from the oven, avoiding spaces free of metal inside the fiber (gaps). A gasket made of PTFE is used to seal the pressure cell.

External pressure from a nitrogen gas bottle is applied inside the cell, and the metal is pumped into the fiber holes. The pressure used is around 1.5 bar. The metal inside the fiber holes solidifies when the fiber exits the oven due to the temperature difference, preventing more metal from being pumped into the fiber. The electrode length is adjusted by the length of the fiber section inside the oven in this first stage. The filling process takes a few minutes (≈ 10 minutes). After filling, the oven is switched off, and it cools down while the pressure inside the cell is kept. After cooling, all the metal inside the fiber solidifies, and the pressure in the cell is removed.

The second stage of the filling involves shifting the metal inside the fiber to keep the ends of the fiber free of metal. Empty ends are necessary for splicing the fiber later in applications. The inner metal container is removed. The tip of the fibers is kept inside the cell. The oven is heated again, and additional fiber free of metal is inserted into the oven. When the oven reaches 160°C, pressure

is applied to the cell shifting the metal inside the fiber. The shifted length is the additional length inserted into the oven in the second stage.

It was noted experimentally that pulling the fiber slowly from the oven in the second stage avoids the formation of gaps (short sections free of metal inside the holes). The speed of the pulling is around 10 cm/minute.

After the two stages of the filling procedure, the fiber has internal electrodes, and it is free of metal on both ends. The electrodes need to be contacted externally by polishing the side holes.

3.4 Electrode contacting

After filling, the fiber with metal is positioned in a polishing setup. The setup consists of a microscope, two rotating fiber holders, a polishing machine, and a soldering iron. A photo of the polishing arrangement can be seen in Figure 3.3.

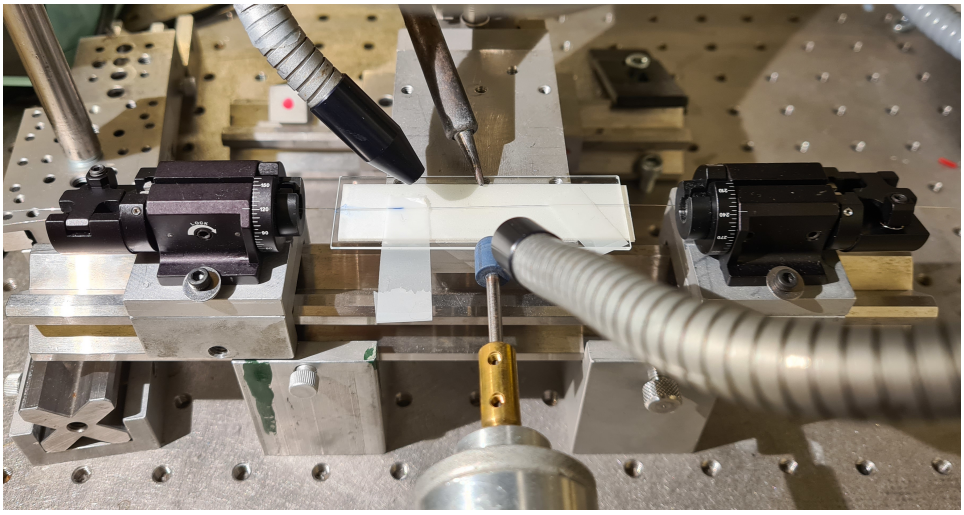

Figure 3.3: Polishing setup showing the rotating fiber holders, the polishing machine, the soldering iron tip, and the microscope base.

The fiber is examined to certify that both holes are filled, and no gaps are formed. A microscope image of the fiber showing both electrodes can be seen in Figure 3.4a.

With the help of the rotating fiber holders, the fiber is rotated until only one electrode can be seen in the microscope, as seen in Figure 3.4b. The fiber is then polished from the side with the polishing machine, exposing the metal (Figure 3.4c.). The soldering iron tip at 230°C is positioned close to the polished area and melts the exposed metal. A thin tungsten wire ($\Phi = 20\mu m$, with Au coating) is inserted into the fiber holes, as seen in Figure 3.4d. After the wire is inserted into

the fiber, the soldering iron is moved out. The BiSn electrode solidifies, creating a bonding between the wire and the electrode inside the fiber. After the metal bonding, a drop of UV curing glue is deposited on top of the exposed electrode with the wire and cured with UV light. The UV glue is used to increase the mechanical resistance of the polished region.

After contacting both electrodes with the thin wire, external devices such as a power supply or voltage generators can be connected to the fiber component, and an electric field can be established in the fiber core.

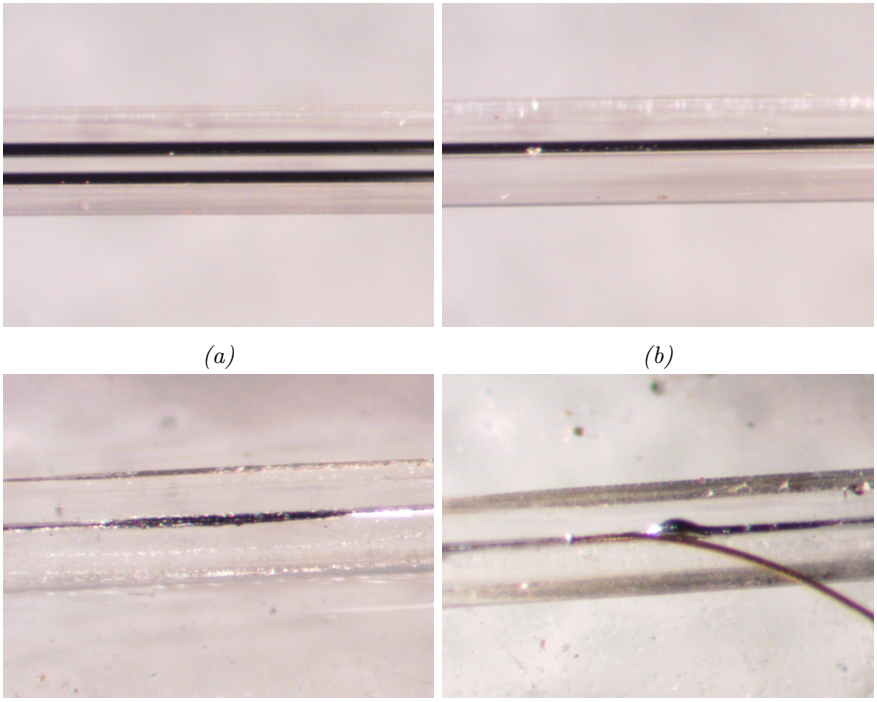

Figure 3.4: Side view of a twin-hole fiber showing the electrodes inside the holes. a) Two electrodes inside the fiber after filling. b) The fiber is rotated, and only one electrode is seen. c) The fiber is polished, and the electrode is exposed. d) A thin wire is inserted into the melted metal.

3.5 Electric characteristics

The internal electrodes of the fiber have an intrinsic resistance and inductance, and they are separated by a silica dielectric forming a capacitor. The equivalent

electrical circuit of fiber with two internal electrodes can be approximated with the circuit of the Figure 3.5.

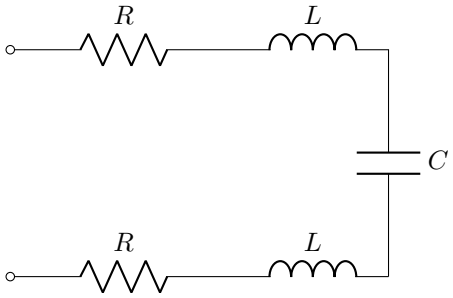

Figure 3.5: Equivalent circuit of a fiber with internal electrodes.

The resistance of the electrodes can be obtained from the resistivity of the alloy used:

$$R = \rho \frac{l}{\pi \left(d/2\right)^2} \tag{3.1}$$

where l is the electrode length and d is the electrode diameter. For the $Bi_{58}Sn_{42}$ alloy used in most experiments a resistivity of $3.8 \times 10^{-6}\,\Omega \cdot \mathrm{m}$ is expected [61]. For comparison the resistivity of copper is $1.68 \times 10^{-8}\,\Omega \cdot \mathrm{m}$.

The inductance of each electrode can be approximated to the self-inductance equation of a straight wire [62]:

$$L = 0.2 \times 10^{-6} l \left(ln \frac{2l}{d/2} - \frac{3}{4} \right) \tag{3.2}$$

The capacitance can be calculated using the relative permittivity of the silica, which is $\epsilon_r = 3.8$ [63], and using the equation for the capacitance of two parallel wires [64]:

$$C = \frac{\pi \epsilon \epsilon_r l}{\operatorname{arcosh}\left(\frac{a}{d}\right)} \tag{3.3}$$

where $\epsilon \approx 8.85 \times 10^{-12}\,\mathrm{Fm}^{-1}$, a is the separation between electrodes (center to center).

For a fiber with electrode diameter of $30\,\mu$m, electrodes separation (edge to edge) of $24\,\mu$m and assuming electrodes length of 1 m, the resistance R is $\approx 538\Omega$, the inductance L is $\approx 2.2\mu$H and the capacitance C is $\approx 88\,$pF.

The electric parameters in an electro-optic fiber component are essential to define the device's speed, electrical power requirements, and operating frequencies. More extended electrodes can make low V_π devices but with a slow rise time.

Short electrodes and low resistivity metal should be used if faster components are the target.

Apart from L and R, which need both ends of each electrode to be contacted, the capacitance is relatively easier to measure with a capacitance meter. Measurements for the capacitance in components made using fibers from Figure 3.1 gave capacitances ranging from 70 - 90 pF for $\approx$ 1 m long electrodes, which is in line with the calculations from Equation 3.3.

The equivalent circuit from Figure 3.5 indicates that the fiber component has a frequency dependency. The resonance frequency can be estimated using the resonance frequency of a RLC series circuit:

$$f = \frac{1}{2\pi\sqrt{LC}} \tag{3.4}$$

For a device with $C = 88$ pF and $L = 2.2\mu$m, a resonance frequency of ≈ 11.4 MHz is expected. A component operating at the resonance frequency is expected to draw more current from the source, and possibly heat would be generated. The rise time for this device $\tau = RC$ is $\approx 47 \times 10^{-9}$ ns when $R = 538\Omega$.

Experiments made to find the resonance frequency gave mixed results. One reason for the difficulties found could be the high resistive electrode that leads to losses when the electrical wave propagates in the electrode. For the rise time, experiments in **Paper IV** showed a rise time of 27 ns for a 60 pF component, which is in the same order of magnitude as the estimated value shown here.

3.6 Optical loss

There are two sources of optical losses in fibers with holes filled with metal: connectorization with other optical components or interaction of the light with the metal electrode.

The connectorization can be made by splicing the fiber to another standard fiber, e.g., an STF fiber from a coupler, or by adding a connector to the fiber tip (e.g., FC, LC, SC). If splicing is the chosen method, losses could be originated from collapsed holes during splicing. Figure 3.6 shows a splice made between a twin-hole fiber and an STF fiber. Figure 3.6a is taken before splice, the two holes of the twin-hole fiber (left) and the core of the STF fiber (right) are seen. After splicing, it is possible to see a slight decrease in the twin-hole fiber diameter, as seen in Figure 3.6b.

When the holes collapse, the core is stretched in a preferable direction, making the core elliptical. The geometry mismatch from the two fibers being spliced create optical losses. The splicer arc duration and power need to be adjusted to reduce the collapse. A frequently used technique is purposely shifting the fibers to concentrate more power on the STF fiber. Splice loss as low as 0.05 dB can be achieved without much effort.

A mechanical splice can also be used, utilizing a cold method. A low-loss splice can also be made because the holes do not collapse. Mechanical splice loss lower than 0.19 dB can be made.

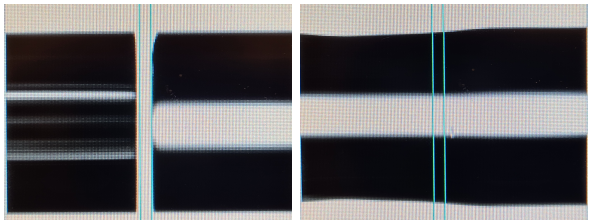

(a) *(b)*

Figure 3.6: Images of fiber with holes (left) and an STF (right). a) Before splicing. b) After splicing, the holes are collapsed, and the diameter of the twin-hole fiber is smaller.

If optical connectors are added to the fiber component, such as an FC connector, the fiber is inserted into a fiber ferrule, glued, and polished. The losses are identical as expected from a connection between standard fibers.

The other source of optical losses is the interaction of the light in the core with metal. If the holes are too close to the fiber's core, the fiber can become lossy when the holes are filled with metal.

Optical losses due to electrode proximity is an inherent problem in electro-optic devices made of thermally poled fibers, where one electrode needs to be very close to the core.

The closer the electrodes are in optical poling, the higher the electric field produced if the same voltage is used. As mentioned before, the fibers used in this work have $\approx 10\,\mu$m clearance from the core. This separation is acceptable to provide a low-loss fiber device, and light interaction with metal is low.

3.7 Poling with light

As discussed in Section 2.5.2, free charges can be displaced if an external electric field is applied while light excites the fiber core. The charges can be frozen if the optical excitation is removed, poling the fiber. Optical poling is used to induce a linear electro-optic effect in the experiments mentioned in this thesis. Two wavelengths were explored: green light (532 nm) from a frequency-doubled Nd:YAG laser launched into the fiber (Figure 3.7a) as studied in **Paper I**, and UV excitation from a tubular lamp by side exposure (Figure 3.7b), as studied in **Paper II**.

Many devices were fabricated using the green light poling method. The light from a frequency-doubled mode-locked (100 MHz) and Q-switched Nd:YAG laser is launched into the fiber to excite the core, releasing charges for poling. The

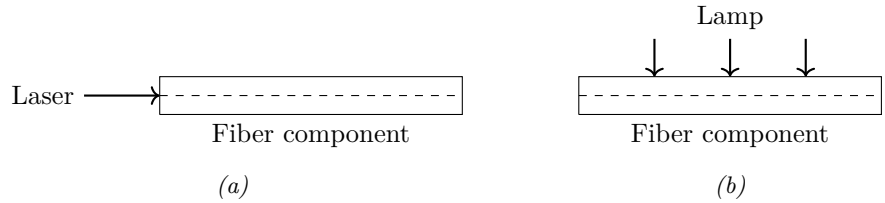

Figure 3.7: Light exposure methods in optical poling. a) Core excited by light coupled into the core. b) Core excited by light from the side

laser operates at 1064 nm, and the light is frequency-doubled with a 3 mm KTP crystal generating 532 nm radiation. The infrared light is removed with a dichroic mirror and a filter to avoid damaging the fiber.

A Q-switch frequency of 1.2 kHz and 3.2 kHz successfully poled fibers, but 3.2 kHz is preferred because the laser operated more stable in this regime. The lower peak energy also decreases the chance of damaging the tip of the fiber during a poling experiment. In this regime, poling over ≈ 20 minutes with 15 mW coupled averaged power is usually enough to saturate the induced nonlinearities, i.e., the recorded field is equal to the poling field. A photo of a piece of fiber being poled with green is in Figure 3.8.

A detailed study of the power and time needed to optically pole fibers was not made, but in **Paper I** it is shown a study where the induced nonlinearity growth is monitored for two different power intensities (17 mW and 8.5 mW) showing saturation after a few minutes. The laser was operating with Q-switching at 1.2 kHz in this case.

In **Paper I**, the green light was also used to erase poling. The process is fast and takes a few minutes. Experiments show that a residual poling field is always present even after erasure.

In **Paper II** the radiation from a tubular lamp was used to pole fibers. It was shown in the literature that a UV laser could pole silicate fibers [58, 59, 65] but an unpolarized and incoherent light source was not explored before. Here the fiber is exposed to UV radiation from the fiber's side, perpendicular to the core, as seen in Figure 3.7b.

The method's advantages are the ability to use a cheap light source and the possibility to pole fibers in parallel, enabling the production of many poled components at once. The disadvantages are that the fiber needs to have the coating removed before the side exposition, and the process can take longer times (≈ 60 minutes) when compared with green poling.

3.8 Stability of optically poled fibers

There are not many reports about the stability of the induced nonlinearities in optically poled fibers. In early studies of optical poling with UV, the stability of

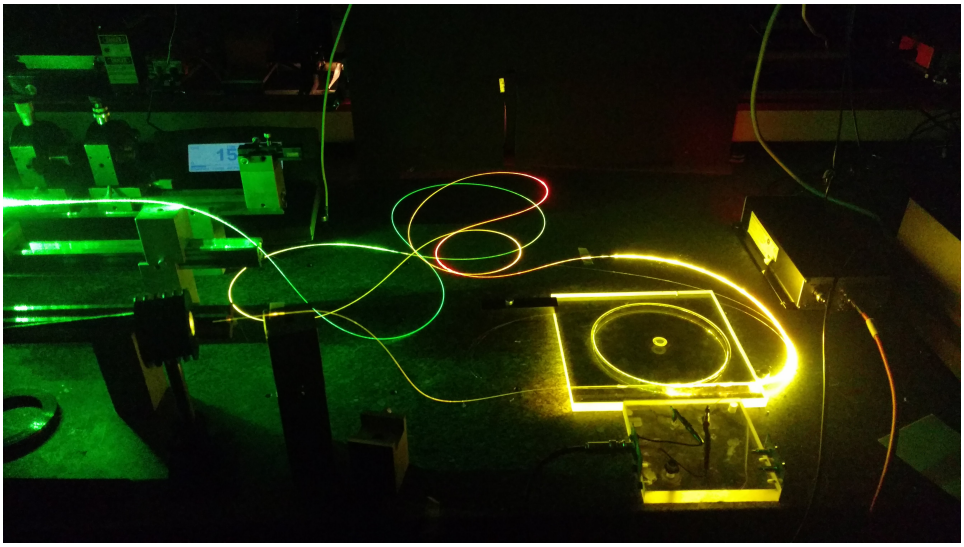

Figure 3.8: Piece of fiber with electrodes being poled with green light.

poling was evaluated, and a time constant of 280 days at 15°C was found [65]. The low time constant can limit potential applications.

Elevated temperatures can accelerate the poling decay process by thermal aging. In **Paper II** the thermal stability of poling with UV lamp is discussed. The study is not complete but indicates that optically poled fiber with a UV lamp is relatively stable over time, in contrast with [65] when a pulsed laser was used.

In **Paper II**, a piece of fiber heated with temperatures up to 130 °C (limited by the melting point of the internal electrodes) for 20 hours showed little decay, as can be seen in Figure 3.9. For temperatures up to 70°C over 60 minutes, no decay was observed, as shown in Figure 3.10.

In the lab, optically poled components with green stored at room temperature could be used in electro-optic experiments after one year without poling decay. The reason why poled fibers with a pulsed UV laser were poor [65] and poled fibers with a green light or with the UV lamp was found to be more stable is not clear.

In Figure 3.9 the experimental points are fitted to a double exponential curve. A fast and a slow decay is also seen in fiber Bragg gratings [66], frequency doubling fibers [67], and thermally poled fibers [68].

It is known that the stability of thermally poled devices is very high, reaching a 10% decay after 1000 hours of treatment at 90°C [69].

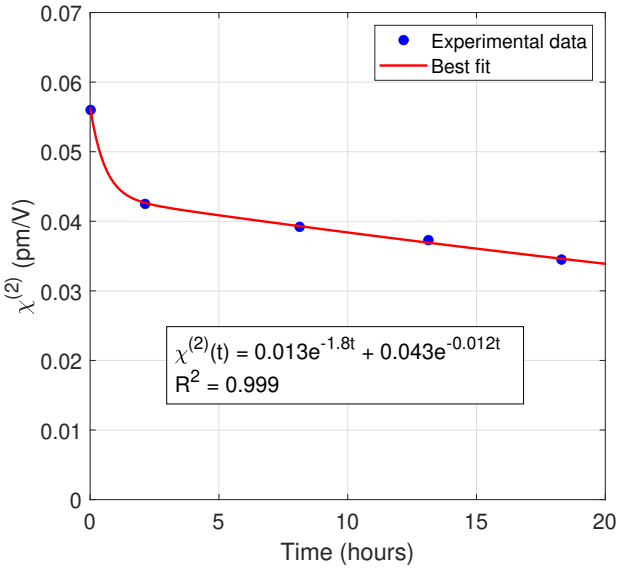

Figure 3.9: Decay of induced $\chi^{(2)}$ over time for a fiber treated at 130 °C for 20 hours. From ***Paper II***

3.9 Polarization dependence

It is expected birefringence in an electro-optic material since the electric field is applied preferably in one direction, as mentioned in section 2.3.1. However, in poled glass [36, 39, 70] and silicate fibers [71, 72] the polarization dependence is weak and $< 15\%$ [4]. The low birefringence is attributed to electrostriction in the glass [36, 39, 71]. The stresses caused by the electric field also create an optical phase delay, the stress-optical effect, in the waveguide. A poled silica waveguide also shows low linear loss (1 dB/cm) and weak polarization-dependent loss (0.2 dB/cm) [70]. Figure 3.11, from [72], shows a piece of a thermally poled fiber showing little polarization dependence when two orthogonal polarization is launched into the fiber.

The low polarization dependence of electro-optic devices fabricated using poled glass components contrasts with the strong polarization dependence found in components used for frequency doubling, as mentioned in [4].

Another source of polarization issues comes from the metal electrodes inside the fiber. If the electrodes are made by pumping molten metal inside the fiber, stress leading to birefringence can be caused if the internal electrodes expand when it solidifies. In [73] an FBG were inscribed in a fiber with electrodes showing a strong birefringence ($B = n_x - n_y \approx 10^{-4}$) when two FBGs separated by 150 pm were created for two orthogonal polarization states, as seen in Figure 3.12.

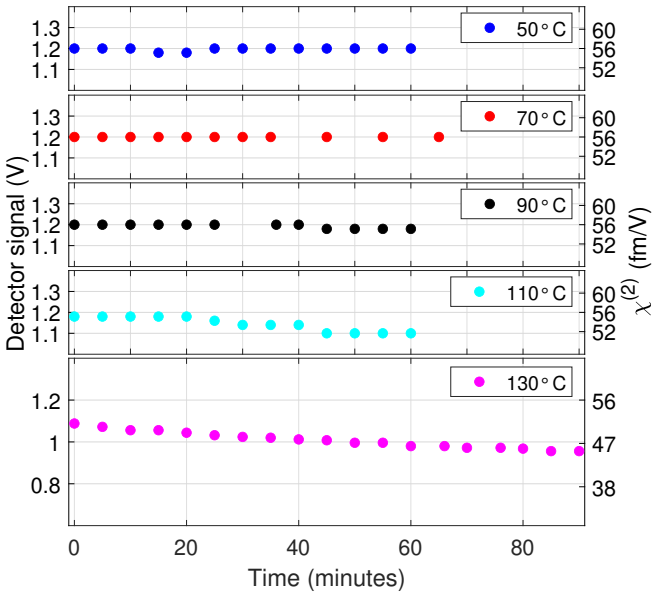

Figure 3.10: Time dependence of the induced nonlinearities for different aging temperatures; on the right axis is $\chi^{(2)}$ in fm/V. From ***Paper II***

In [47] a numerical study was made to evaluate the birefringence caused by the expansion of BiSn alloy in the fiber. It was found that the expected birefringence could be as high as $\approx 2 \times 10^{-4}$ if the metal expands radially inside the holes. This number is similar to the value found in [73], but it differs from values found in [74] of $< 4 \times 10^{-5}$. In the latter, the explanation was that the metal solidifies and expands along with the fiber instead of creating radial stress. For the experiments shown in [73] the explanation could be linked to the pulling mechanism shown in Figure 3.2. Since the fiber is being moved out from the oven and a sudden temperature difference is expected along with the fiber (inside the oven is ≈ 160°C and outside is ≈ 25°C), the solidification of the metal could be expanding more radially than longitudinally.

Polarization dependence and acoustic resonance are concerns in electro-optic devices. A polarization-independent electro-optic component is an advantage for applications in optical communication, such as phase and amplitude modulators. The birefringence caused by the internal electrodes seen in Figure 3.12 ($B = n_x - n_y \approx 10^{-4}$) can be avoided if different alloys were used during the filling process. Nevertheless, the birefringence could be exploited in polarization control applications.

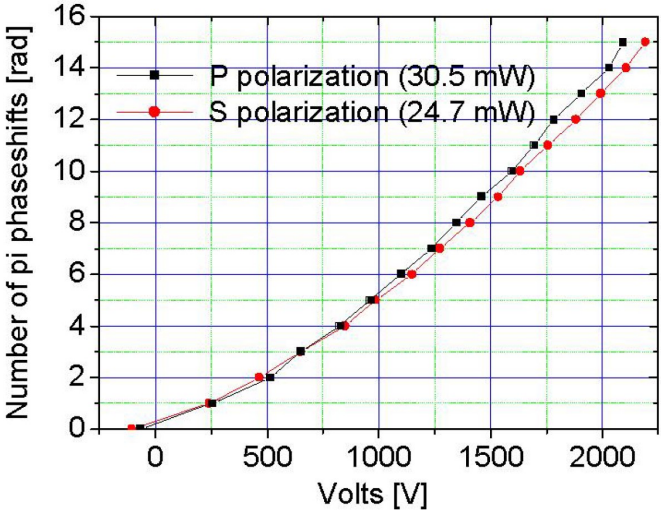

Figure 3.11: Phase shift for orthogonal polarization with applied voltage in a 70-cm long thermally poled fiber, showing little polarization dependence. From [72].

3.10 Characterization of induced nonlinearity in poled fibers

Characterization methods to quantify the induced nonlinearities in poled fibers are usually made by measuring the SHG or the electro-optic effect. Complementary information such as the electric field distribution can be obtained by SHG microscopy and etching. With etching an image of a frequency doubling grating generated along an optically poled fiber could be taken [75]. The spatial charge distribution in the core of an optically poled fiber is complex due to the small dimensions ($< 10\mu$m) and the relatively weak second-order nonlinear coefficient induced.

For SHG measurements, the internal electrodes of the fiber are in some cases removed. However, in electro-optic measurements, the electrodes are used to bias the media, and the phase delay can be monitored usually in an interferometric setup.

Since the focus of this thesis is on electro-optic components, SHG measurements were not evaluated.

3.11 Electro-optic characterization

The Sagnac interferometer was the main method used to characterize active fibers in the experiments of this thesis. Figure 3.13 shows the interferometer used with

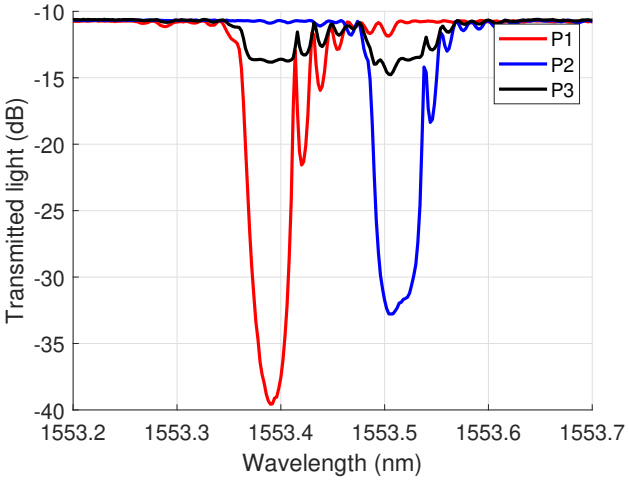

Figure 3.12: Polarization dependence is seen in an FBG inscribed in fiber with internal electrodes. For polarization P1, the polarization was maximized to 1553.4 nm. For polarization P2, the maximized wavelength was 1553.5 nm, and on Polarization P3, the polarization controller was adjusted for equal intensities. From [73].

its main components. The polarization controller maximizes the signal while the photodetector output is monitored with an oscilloscope.

Typical oscilloscope traces captured using the Sagnac interferometer from Figure 3.13 can be seen in Figure 3.14. Red (left axis) represents the applied voltage to the fiber electrodes, and blue (right axis) is the optical intensity measured with the photodetector. The voltage pulses biasing the fiber have a 400 ns pulse width with a repetition rate of 1 kHz, generated with a fast HV switch. The two pulses seen in the blue trace are due to the different optical paths of the Sagnac interferometer (clockwise and anti-clockwise). The separation in time between pulses is related to the fiber delay added to the setup. The optical pules intensities vary between a maximum and a minimum value depending on the voltage bias. V_π is the voltage needed for total intensity excursion, as discussed in the Section 2.3.1. The contrast can be maximized with the help of the polarization controller. Suppose the intensities of the optical pulses for incremental voltage bias are recorded. In that case, it is possible to create an interferometric pattern curve that can be used to characterize the active fiber component, as discussed in the Section 2.6.

If a piece of fiber with electrodes is characterized before poling, it is expected to have a symmetric and quadratic dependence, as seen in Section 2.3.2. Figure 3.15 shows an interferometric curve obtained with the Sagnac interferometer from Figure 3.13. It shows that the curve is symmetric around zero, and V_π of $\approx$ 1900 V and $\approx$ -1900V are obtained. With the measurements, it is possible to calculate

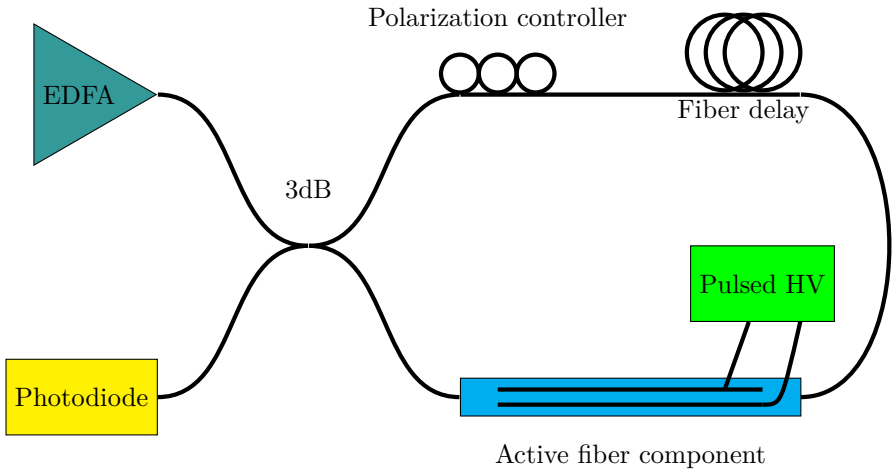

Figure 3.13: Sagnac interferometer used to characterize the electro-optic effect in silicate fibers.

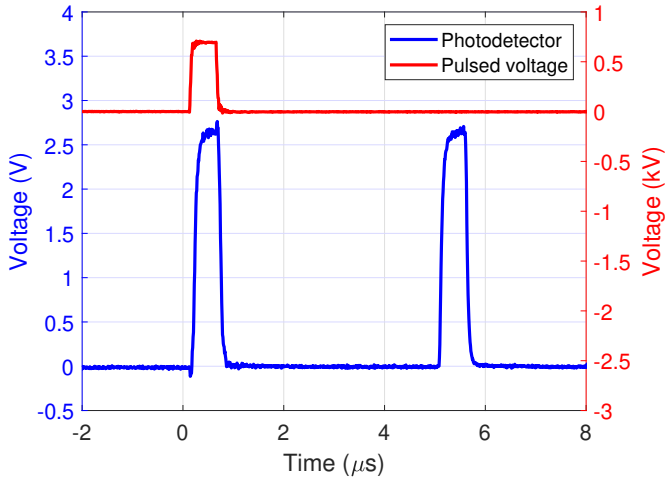

Figure 3.14: Typical oscilloscope traces with the pulsed applied voltage on the active fiber (red) and the optical pulses (blue) measured with the photodetector. From ***Paper II****.*

the third-order nonlinear coefficient, $\chi^{(3)}$, for silica. For the data in Figure 3.15 a fitting curve using Equation 2.20 gives $\chi^{(3)} = 2.02 \times 10^{-22}\,\mathrm{m^2/V^2}$, very close to the expected value of $2 \times 10^{-22}\,\mathrm{m^2/V^2}$ [76].

If a fiber with the same characteristics is poled, an internal electric field is

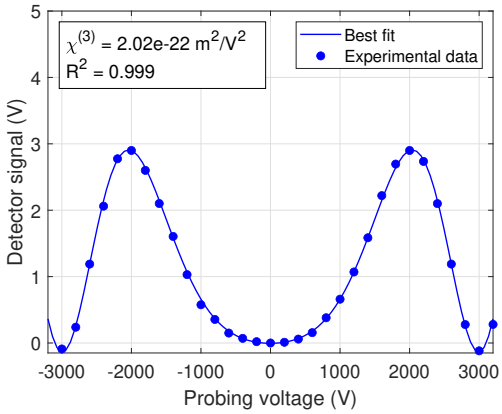

Figure 3.15: Interferometric measurement using an electro-optic fiber. The signal measured is the transmitted light intensity in a Sagnac interferometer. $V_\pi \approx \pm 1900V$. From ***Paper V****.*

frozen, and a non-symmetric pattern is expected. In Figure 3.16 it is shown an electro-optic characterization of a poled fiber. It is evident that the fitted curve is not symmetric around $V = 0$ V. V_π is reduced to ≈ 330 V, much lower than $V\pi \approx 1900V$ for fiber without poling.

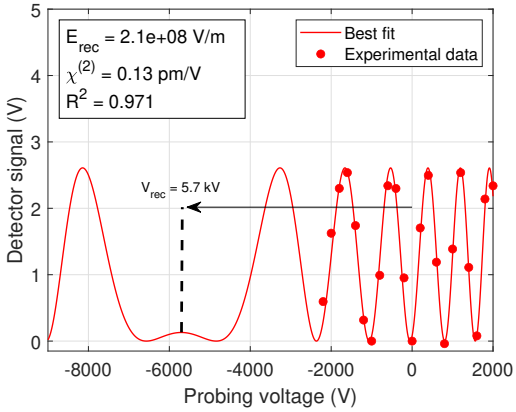

Figure 3.16: After poling, the fiber has different behavior, and the symmetry around 0 volts changed. The first V_π is around 330 V. From ***Paper V****.*

It is easy to quantify and visualize the recorded field frozen in the fiber from the interferometric measurements. In Figure 3.16, the symmetry of the interferometric curve is restored when $V = -5.7$ kV. Applying $V = -5.7$ kV in the

electrodes cancels the internal field created with poling. If the separation of the electrodes is 24 μm, the field recorded E_{rec} is $\approx 2.4 \times 10^8$ V/m (using the approximation $E = V/d$). The results presented in Figure 3.16 utilize a correction for the electric field due to the electrode curvature [76], and E_{rec} is calculated to be 2.1×10^8 V/m. The electric field correction is based on a numerical study of the electric field in the core when rounded electrodes are used. The study gives a correction parameter to the approximation $E = V/d$, based on the electrode separation and the diameter of the electrodes in a symmetric fiber. Figure 3.17 shows the relative error of the approximation $E = V/d$ for a relation between the separation and the holes diameter.

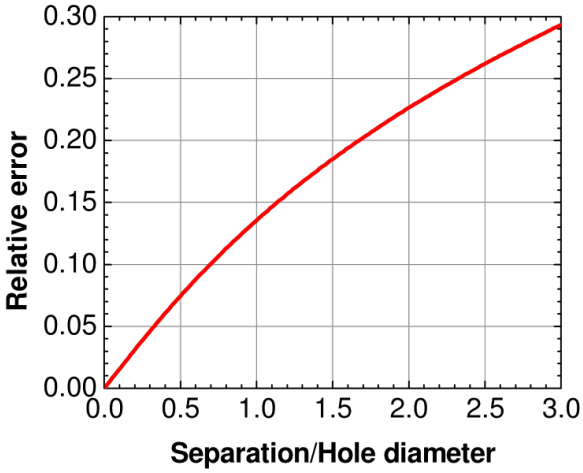

Figure 3.17: Relative error by using a parallel plate approximation to calculate the electric field in the core center. From [76].

Similar to the case before poling, the curve after poling can also be fitted using the Equation 2.20, giving the value for the induced $\chi^{(2)}$.

Chapter 4

Summary of included papers

This chapter presents a short description of the papers included in this work. Paper I describe the basis of the optical poling experiments. Papers II and V explore different optical poling configurations, and papers III, IV, and VI explore different electro-optic experiments made with poled fibers, showing potential applications.

4.1 Paper I: Optical creation and erasure of the linear electrooptical effect in silica fiber

This paper presents a study of optical poling with a high-power green laser in twin-hole optical fiber with internal electrodes. As mentioned in Section 2.4, charges released with light are displaced by an external electric field and are frozen when the light excitation is blocked.

A frequency-doubled Nd:YAG laser was used for the experiments, and the poling light wavelength was 532 nm. The laser was Q-switched at 1.2 kHz and mode-locked at 100 MHz. The experiments show that the recorded field is limited to the field applied during poling, which was 1.2×10^8 V/m, also noted in [17]. The induced second-order nonlinear coefficient achieved was $\chi^{(2)} \approx 0.06$ pm/V, which is in the same order of magnitude as what is obtained with thermal poling encouraging future work with the technique presented. It was also presented that high-power green can erase the induced nonlinearity, which contrasts with what is reported for blue radiation [77, 78] in studies of optical poling. The paper presents a simulation of the electric field distribution expected inside the fiber before poling, during poling, and after poling.

A free space Sagnac interferometer was built to characterize the induced electro-optic effect during poling. The interferometer used an Erbium-Doped Fiber Amplifier (EDFA) as a probing light source. The experimental setup for poling and electro-optic characterization is shown in Figure 4.1.

The fiber used had holes separated by 25 μm, and the electrode length was 25 cm. Electrodes are made by filling the holes with BiSn alloy as explained in

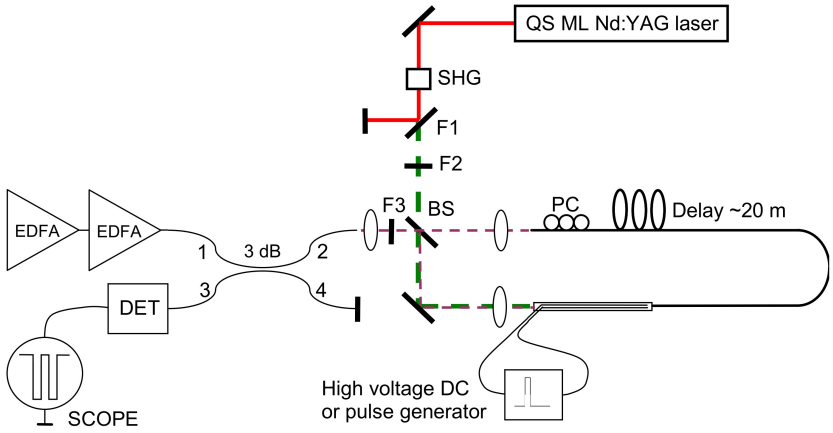

Figure 4.1: The Experimental setup used for optical poling and erasure with green light from a frequency-doubled Nd:YAG laser. It is also shown the Sagnac interferometer used to characterize the induced and erased linear electro-optic effect. From ***Paper I****.*

Section 3.3. Before poling, the electro-optic fiber component had a V_π of 1600 V. Poling was made with 3 kV bias, and an induced $\chi^{(2)}$ of ≈ 0.06 pm/V was seen.

Two different average powers from the laser were used during poling: 17 mW and 8.5 mW, showing that higher power light can pole faster, but the induced nonlinearity saturates at the same level, as shown in Figure 4.2.

Erasure was done by disconnecting the electrodes from the fiber and using the same green light used for poling. The experiment shows that erasure is much faster, and the component can be erased in less than one minute, but a residual poling is still present after a long time of exposure, as seen in Figure 4.3.

The paper shows that high-power pulsed green light can pole fibers and erase the induced nonlinearity. The results show that a fiber made out of a standard telecom fiber can be used for optical poling, and no additional doping is needed. No need for additional doping is a significant advantage because the fibers can be cheaper to fabricate. Since the electrodes are far from the core low-loss electro-optic device can also be fabricated, many applications can take advantage of this, such as quantum communication experiments and electro-optic modulation. The induced effect is not groundbreaking when compared to thermal poling, which can reach $\chi^{(2)} \approx 0.2$ pm/v [79], but it is a clear indication that more experiments can be done to increase the effect.

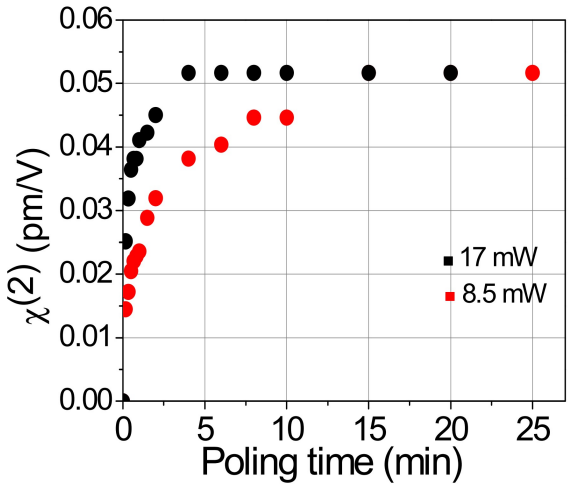

Figure 4.2: Poling time for two different averaged power of green light coupled into the fiber. Higher power saturates the induced effect quicker, but saturation is seen in both cases. From ***Paper I****.*

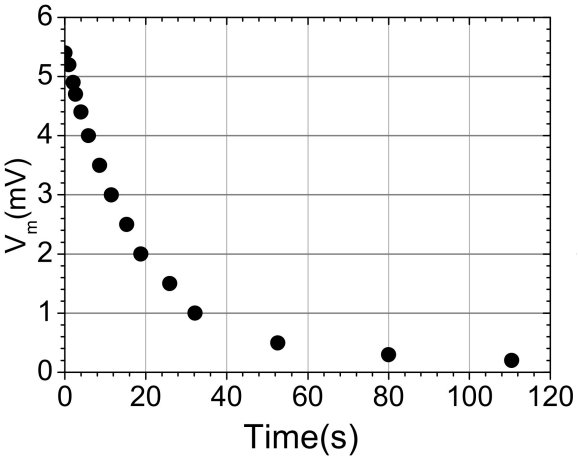

Figure 4.3: Erasure of the linear electro-optic effect induced with poling. The fiber electrodes were disconnected while green light excited the core. From ***Paper I****.*

4.2 Paper II: Linear electro-optical effect in silica fibers poled with ultraviolet lamp

This paper shows that a UV lamp can pole silicate fibers. Optical poling is usually done with high-power lasers, as it is shown in **Paper I** where a frequency-doubled Nd:YAG laser is used ($\lambda = 532$ nm). In [77] pulsed blue light from a dye laser operating at 485 nm and a CW argon laser operating at 488 nm successfully poled fibers. In [59] it is shown a ArF laser ($\lambda = 244$ nm) used for poling and in [58] a 193 nm laser were used.

The fact that low-power, incoherent, and unpolarized light sources can pole fibers shows that simplified and energy-efficient poling methods can be explored. Since the light intensity is lower when compared to laser sources, longer times are needed for efficient poling (≈ 1 hour). Nevertheless, since the fibers are poled by side exposure, as shown in Figure 3.7b, the method can pole many fibers in parallel, optimizing the time. In a side exposure configuration, core alignment is also not needed. In summary, the technique presented in **Paper II** is a good candidate for the production of optically poled devices.

For the experiments, a twin-hole fiber with 40 μm separation between holes (Figure 3.1a) and 1.32 m long electrodes made with BiSn alloy was used. The piece of fiber was placed ≈ 7 mm apart of a UV tubular lamp and had its coating removed. For electro-optic characterization, a Sagnac interferometer, similar to the interferometer shown in Figure 3.13, was built.

The lamp is an Osram HNS 55W [80] and it is 87 cm long. It emits a broad UV spectrum (200-280 nm) with its maximum intensity peak at 254 nm. It is commercialized for UV disinfection, and it is relatively easier to find in the market.

Different poling voltages and poling times were used. For a sample poled with 7 kV, the nonlinearity obtained was 0.062 pm/V, as shown in Figure 4.4. The induced effect is very similar to that achieved with green light poling presented in **Paper I**.

Erasure with a UV lamp was also evaluated, and a slow decay was observed. Figure 4.5 shows the transmitted light intensity measured with the photodetector from the Sagnac interferometer. When pulsed voltages were applied to the fiber electrodes, a change in light intensity was observed in the photodetector. The peak intensities were monitored in real-time with UV exposure.

A study of thermal stability was also made, and it is summarized in Section 3.8. It shows that the induced nonlinearity is relatively stable. Temperatures up to 130°C were used, showing little decay.

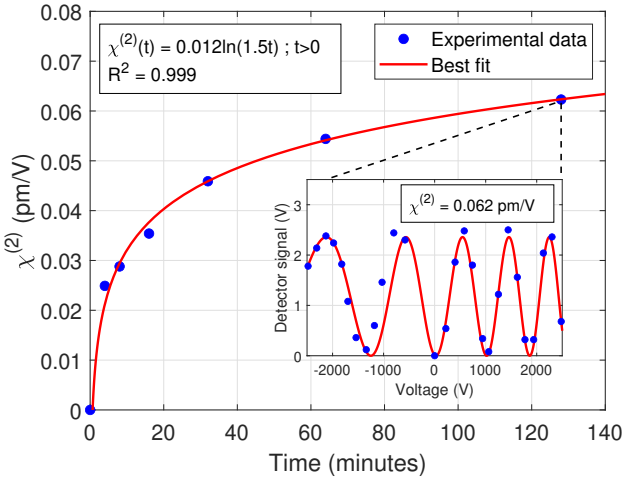

Figure 4.4: Poling time for a sample poled using the UV lamp and 7 kV bias. From ***Paper III****.*

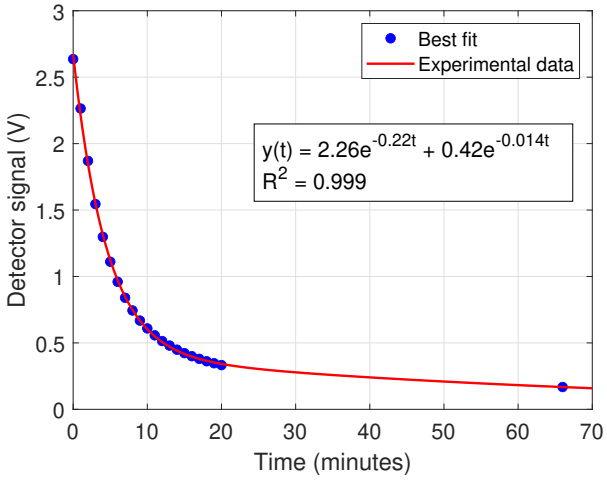

Figure 4.5: Decrease of the induced electro-optic effect by exposure with the UV lamp. From ***Paper III****.*

4.3 Paper III: Towards Distributed Measurements of Electric Fields Using Optical Fibers: Proposal and Proof-Of-Concept Experiment

Paper III explores a possible application of poled fibers in distributed sensing. The work was realized in collaboration with Universidad de Alcalá, in Spain. The method uses an electro-optic fiber component with a highly sensitive Chirped-Pulse Phase-Sensitive OTDR (CP-ϕOTDR) prototype.

CP-ϕOTDR is a Rayleigh based OTDR [81]. It sends chirped pulses into the optical fiber and an advanced algorithm analyses the reflected Rayleigh signal recovering fluctuations in the refractive index. The refractive index perturbation is usually caused by changes in temperature and strain. CP-ϕOTDR has a spatial resolution ≈1-m resolution and can detect perturbations in mK or sub-nε range with interrogation speed of kHz over a distance up to 100 km [82]. This paper explores the use of the technique to measure changes in the refractive index caused by the electric field in silicate fibers. A non-poled and a poled fiber are used.

The CP-ϕOTDR prototype used in the experiments had a sensitivity of $\approx 10^{-9}\Delta n/\sqrt{\text{Hz}}$. The optical pulses were 40 ns linearly chirped with 4 m spatial resolution. The sampling rate was 1 kHz. Two electro-optic experiments were realized with two different fibers. The first experiment evaluates the Kerr effect in a non-poled fiber, and another experiment measures the induced Pockels effect in a thermally poled fiber. For the non-poled fiber, a twin-hole fiber with 40.4 μm separation between holes was used, similar to the fiber shown in Figure 3.1a. The fiber was prepared for this experiment and had 3-meter-long metal electrodes in its holes. The thermally poled fiber was already available in the lab, had 25.4 μm electrodes separation, and had 75 cm long electrodes. The induced $\chi^{(2)}$ was $\approx 0.272\times$ pm/V.

A sinusoidal voltage signal was applied to the fiber electrodes in the experiments, and the refractive index changes were monitored with the CP-ϕOTDR prototype. The calculated refractive index with the applied electric field can be seen in Figure 4.6 for the non-poled fiber and Figure 4.7 for the poled fiber. The results clearly show that the non-poled fiber exhibits a quadratic response and the poled fiber a linear response.

With post-processing and fitting, the value of the third order nonlinear coefficient $\chi^{(3)} \approx 2.5 \times 10^{-22}\,\text{m}^2/\text{V}^2$ was infeered for the non-poled fiber and $\chi^{(2)} \approx 0.27\,\text{pm/V}$ for the poled fiber. The numbers are in reasonable agreement with the expected values of $\chi^{(3)} \approx 2\times10^{-22}\,\text{m}^2/\text{V}^2$ and $\chi^{(2)} \approx 0.272\,\text{pm/V}$ respectively, despite the components being shorter (3 m and 0.75 cm) than the spatial resolution of the prototype (4 m).

The proof-of-concept experiments show that it is possible to quantify electric field changes in the fiber with the CP-ϕOTDR technique. The proposed experiment could find applications in distributed electric field measurements over long distances. Examples are in power plants and transmission lines. Nevertheless,

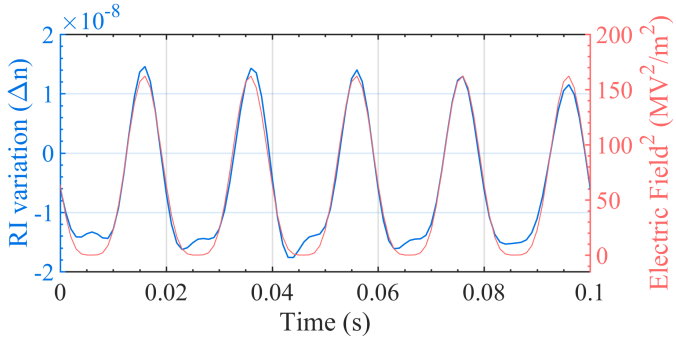

Figure 4.6: Refractive index variation in a non-poled fiber for a sinusoidal 50 Hz electric field modulation, showing a quadratic response. From ***Paper III****.*

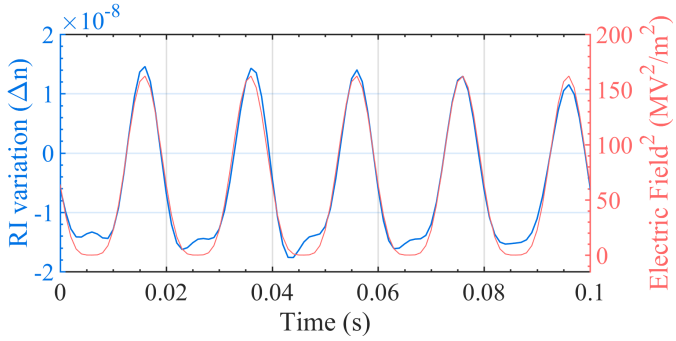

Figure 4.7: Refractive index variation in a poled fiber for a sinusoidal 50 Hz electric field modulation, showing a linear response. From ***Paper III****.*

long-distance poling is still a challenge to be addressed. Also, metal electrodes are usually not wanted in high electric field monitoring applications. External electrodes combined with a poling method exploring side exposure, as mentioned in **Paper II**, from where the fiber can be scanned over long distances, could be a potential solution.

4.4 Paper IV: Electrooptic control of the modal distribution in a silicate fiber

This work describes the report of electrooptic intermodal interference in optical fibers with internal electrodes. As shown in Section 2.2.2, the guided spatial modes propagate at different speeds. The difference in phase of the modes causes intermodal interference that can be modulated by an externally applied voltage to the electrodes.

Two fibers were used in the experiments: one with 40.8 μm and another with 24.4 μm electrodes separation (Figure 3.1). The fibers are single-mode at 1550 nm. When operated at 633 nm, the fiber is multimode, supporting six polarization degenerated modes, as seen in Figure 2.2. The experiment was done by launching two or more modes into the fiber and evaluating the perturbation effect in the mode profile after a propagating distance. Optically poled fibers with green light, using the procedure documented in **Paper I** were used, as well as a non-poled fiber to explore the differences.

Simulations were carried out and showed that the largest effect of a uniform external perturbation over 1 m of the fiber is when LP_{01} and LP_{02} modes are propagating in the fiber, as seen in Figure 4.8.

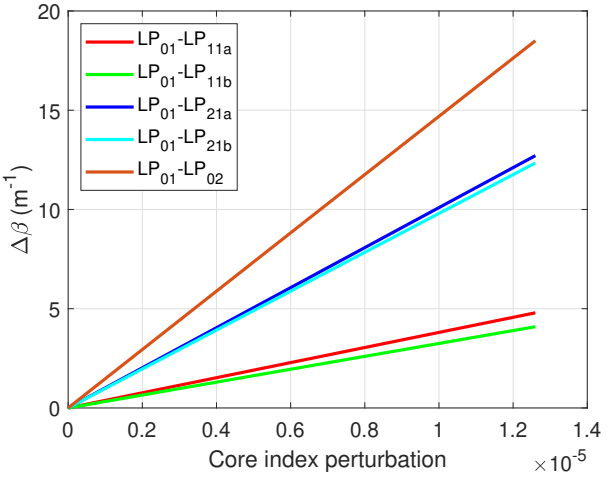

*Figure 4.8: Difference in the propagation constant between modes. The largest effect is for modes LP_{01} and LP_{02}. From **Paper IV**.*

If 50% of the light is in mode LP_{01} and 50% in mode LP_{02}, total extinction is observed in the center of the resulting interference. Figure 4.9a presents a profile line of the transmitted intensity profile. If the intensity of the light is monitored in the center of the mode and higher perturbation is applied, a periodic dependence is seen, as shown in Figure 4.9b. An important observation in the simulations is

that even for a small amount of energy travelling in the LP_{02} mode, as low as 0.5%, can give a contrast as high as 30%.

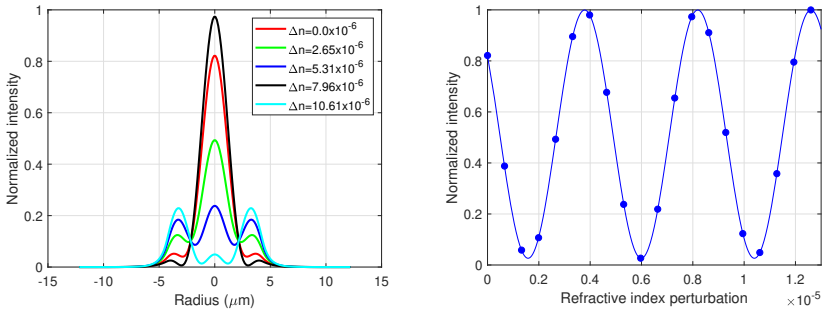

(a) *(b)*

Figure 4.9: a) Profile lines for different uniform index perturbations when modes LP_{01} and LP_{02} are equal in power. b) Intensity at the center of the resulting modal interference between LP_{01} and LP_{02}, showing a periodic response when a uniform index perturbation is applied. From ***Paper IV****.*

In the experiments, the perturbation in the refractive index is caused by voltage changes applied to the fiber electrodes. The light was launched into the fiber in free space, and different modes could be launched into the fiber by changing the alignment.

Figure 4.10 shows the measured mode profile obtained for different voltages applied to the electrodes of the poled fiber. Figure 4.11 shows the periodic response of the interference, as predicted by the simulation.

The experiment shows a contrast of 30%. According to simulations, this means that $\approx 99.5\%$ of the light coupled travels in the LP_{01} and $\approx 0.5\%$ in the LP_{02}.

For the non-poled fiber, the experiments did not show a considerable change in the modal profile.

Experiments show nanosecond response time with a rise time of 27 ns. The paper's results motivate the design of a fiber that guides a few modes at 1550 nm. The new fiber can simplify the methods used in the experiments by using standard telecommunication components. Better coupling of modes can also be made using photonic lanterns [83]. The technique explored may be used for voltage sensing, quantum information, and telecommunication.

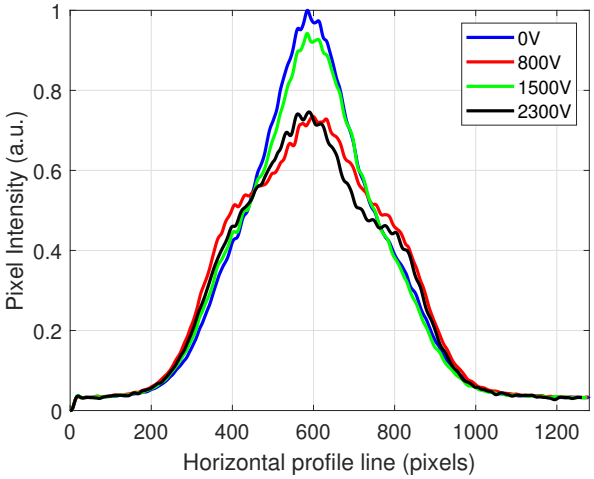

Figure 4.10: Mode profiles for different voltages applied to the fiber electrodes. From ***Paper IV****.*

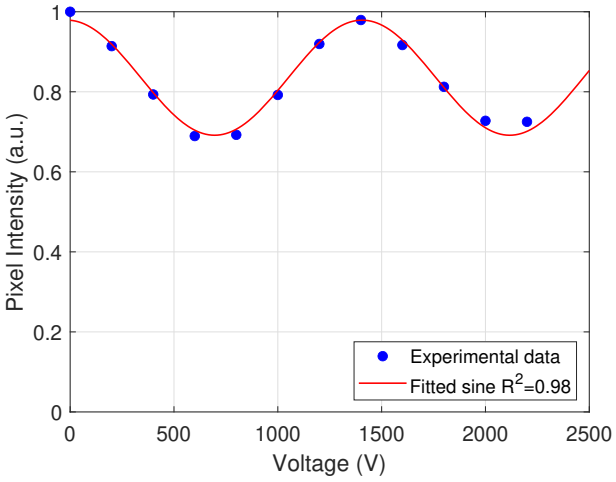

Figure 4.11: Periodic response when the light intensity is measured in the center of the mode. From ***Paper IV****.*

4.5 Paper V: Optical poling by means of electrical corona discharge

In **Paper V** another optical poling method is evaluated. The motivation is to increase the nonlinearity obtained with green poling in **Paper I** and UV lamp in **Paper II**. As seen in previous experiments, the limiting factor for optical poling is the electric field applied in the core during poling [17].

In a conventional optical poling configuration, high voltage is applied to the internal electrodes of the fiber using a power supply. The dielectric strength of the silica limits the voltage. In an eventual electrical breakdown (arcing), the electrical current provided by the power supply can trigger an avalanche effect damaging the fiber. If the mobility of the charges creating the poling field is lower, a catastrophic effect could be less prone to happen.

The corona discharge method described here takes advantage of the limited charges deposited at the fiber's surface to create the poling field. The limited charges decrease the probability of breakdown.

Figure 4.12 shows a numerical study of the electric field inside the fiber when uniform -15 kV is applied to the fiber's surface. One electrode is grounded, represented with the letter "G," while the other is kept at a floating potential. In Figure 4.13 a line is taken crossing the center of the fiber showing the electric field and the electric potential.

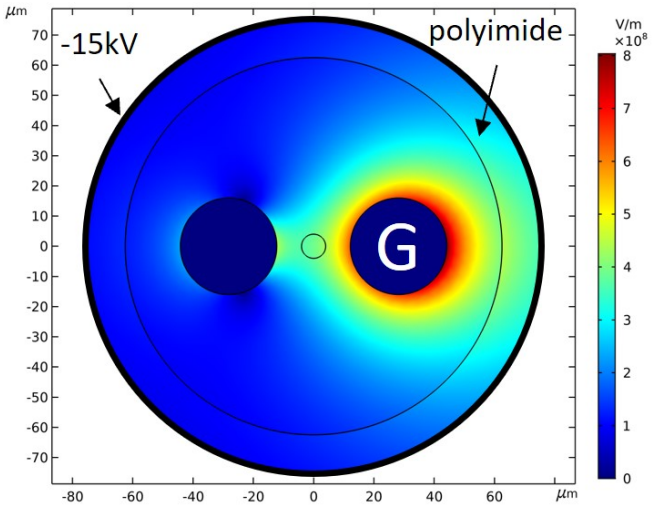

Figure 4.12: Field distribution in the fiber when -15 kV is uniformly distributed on the fiber's surface. One electrode is grounded "G," and the other is kept at a floating potential. From ***Paper V****.*

The paper describes the first reported use of electrical corona discharge to

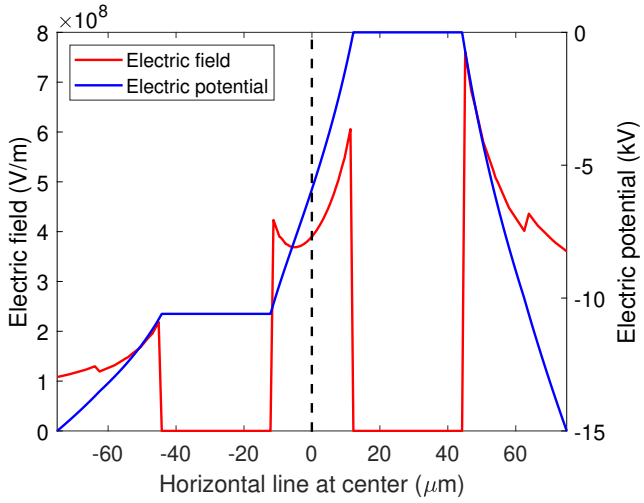

Figure 4.13: Electric field and potential from a line crossing the center of the fiber. The electric field in the core is $\approx 3.9 \times 10^8$ V/m *for -15 kV uniformly distributed on the fiber's surface. From* ***Paper V****.*

electrostatically charge an optical fiber and create a strong electric field at the fiber core. The field is used to displace mobile photocarriers generated with green laser light, poling the fiber. The poling with green used is similar to the experiment done in **Paper I**. The fiber used (Figure 3.1b) was polyimide coated instead of acrylate to provide thin and strong insulation. The fiber had 0.57 m electrode length.

A thin tungsten wire $\approx$ 9.5 cm from the fiber was biased with -15 kV to generate the corona ions. The typical blue color from a corona discharge is seen in Figure 4.14.

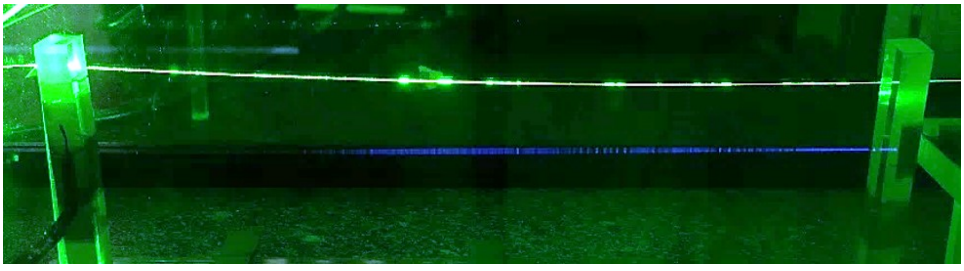

Figure 4.14: Photo of the corona discharge for the poling experiment. A thin tungsten wire was biased with -15 kV ionizing the air. Green light from the frequency-doubled Nd:YAG was launched into the fiber for poling. From ***Paper V****.*

Only 37 cm of fiber with electrodes were directly exposed to corona charges. After $\approx$ 20 minutes of ionization, green light from the Nd:YAG laser was launched into the fiber, and the fiber was poled for $\approx$ 20 minutes. After the poling time, the light was blocked, and the voltage biasing the tungsten wire was removed.

The highest second-order nonlinear coefficient measured was 0.13 pm/V. A significant increase of the coefficient reported in **Paper I** ($\chi^{(2)} \approx 0.06$ pm/V) and **Paper II** ($\chi^{(2)} \approx 0.062$ pm/V). Experiments also shows that corona ionic distribution is a slow process.

The corona experiments show that higher nonlinearities can be obtained with optical poling. The induced effect is comparable with thermal poling with the advantage of being a low loss component. The experiment can be improved in many ways, starting from the length of fiber directly exposed to the corona discharge and better control of the processes involved in the corona discharge (gases, pressure, humidity, among others).

4.6 Paper VI: Voltage sensing using poled fibers and FBG

This paper is a collaboration with Universitat Politècnica de València. In this work, a Bragg grating is inscribed in a twin-hole fiber with internal electrodes. The FBG is used to measure variations in the refractive index due to the electric field. The electric field is applied to the fiber by applying voltage to the internal fiber electrodes. For the experiments, a non-poled fiber and a poled fiber were used.

Changes in the refractive index due to electric field shifts the Bragg wavelength to the right or to the left.

For AC measurements, a tunable laser light source was adjusted to the FBG slope, and the reflected signal intensity was measured with a photodetector. The wavelength shift change the light intensity monitored. The interrogation system used is shown in Figure 4.15.

For DC measurements a commercial interrogator with 1 pm resolution was used.

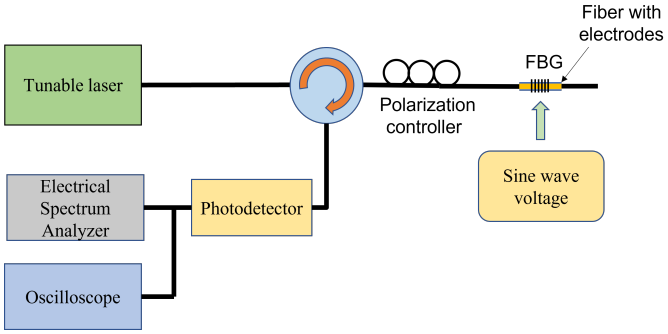

Figure 4.15: Diagram of the interrogation system used in the experiments. From ***Paper VI****.*

A sinusoidal waveform up to 1 kV was applied to the fiber electrodes, and the detected intensity was monitored. For the non-poled fiber, only the Kerr effect is expected. Figure 4.16 shows the photodetector intensity variation for the voltage applied. It shows a quadratic dependence with the applied voltage. DC measurements with the non-poled using the commercial interrogator was difficult to measure.

After poling a fiber sample with 5 kV for $\approx$ 20 minutes and repeating the experiments, the photodetector intensity changes with voltage shows a linear response, as seen in the Figure 4.17.

The experiments are still in progress, but it shows that an experiment using FBGs to measure the electro-optic effect in silicate fibers can be explored. The method's advantage is using a single-ended monitoring technique to measure changes in the electric field. It also makes possible the implementation of

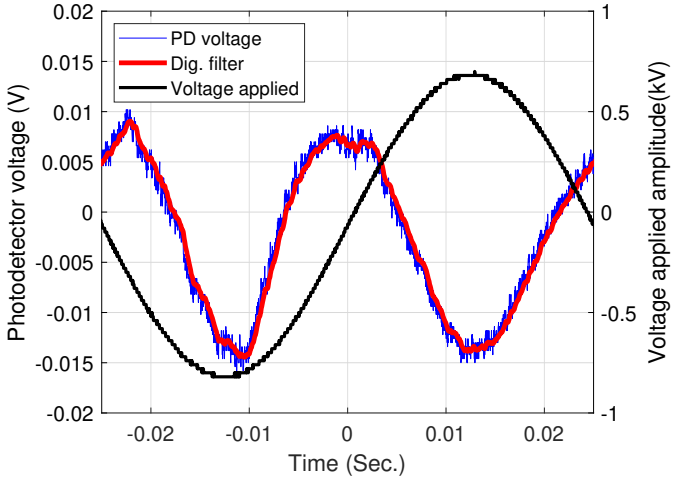

Figure 4.16: Light intensity measured for changes caused by a voltage modulation applied to the fiber electrodes. The fiber was not poled. The applied voltage had an amplitude of 750 V and a frequency of 50 Hz. A quadratic response is seen. From ***Paper VI****.*

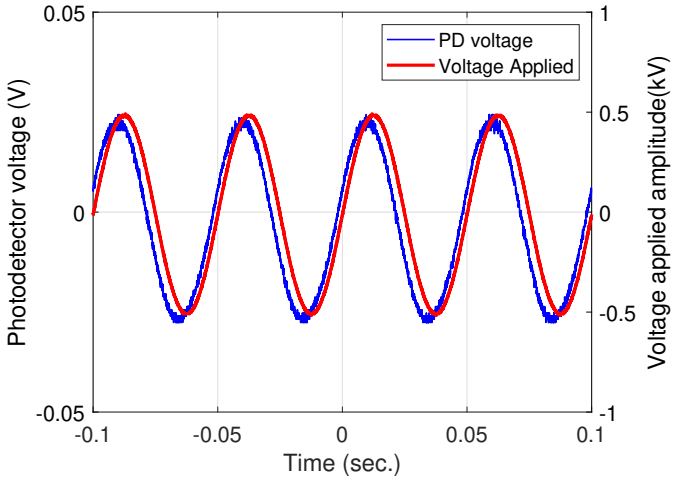

Figure 4.17: Light intensity measured for changes caused by a voltage modulation applied to the fiber electrodes. The fiber was poled with green light from a Nd:YAG laser with 5 kV. The applied voltage had amplitude of 1 kV and frequency of 50 Hz. A linear response is seen. From ***Paper VI****.*

a multi-point and multi-parameter sensing device. Commercial FBG interrogators can also be explored, simplifying the measurements and enabling potential applications.

Chapter 5

Conclusions

The work presented in this thesis shows the recent progress of our group in optical poling. It also shows electro-optic experiments with potential applications of poled fiber components.

Paper I is the basis of the optical poling experiments carried out. It shows that a frequency-doubled Nd:YAG laser can be used to free charges in the fiber core. The charges are displaced by an external electric field and are frozen when the light is blocked. The method enables poling at room temperature, and the fibers can be made using standard telecommunication fiber preform. The study motivated work in optical poling.

Paper II Explores a new light source for poling. The motivation was to study UV poling and find potential poling methods that could be explored in multiple poled device fabrication. The method uses a cheap UV tubular lamp to excite the fiber core for poling. One disadvantage of the method is the removal of the coating before poling. However, the fibers could be poled in a fiber draw tower before the coating process.

After exploring different light sources, the focus went to optimizing the electric field used for poling. It was seen that the limiting factor for optical poling is not the light source or the number of freed charges in the core, but the field applied during poling [17]. The higher the field, the higher the induced nonlinearities. The electric breakdown in the silica limits the electric field. For the fibers tested, the maximum applied voltage was $\approx$ 10 kV for a short time. Poling periods of $\approx$ 20 minutes were consistent and reliable with voltages up to 6 kV.

Paper V uses corona discharge to create a charge distribution on the surface of the fiber. The ionized charges are attracted to the fiber because one electrode is grounded. The electric field created inside the fiber is used for poling with green light. The low mobility of the ionized charges could prevent a breakdown from occurring. The results showed an induced nonlinear coefficient of $\chi^{(2)} \approx 0.13$ pm/V, good progress when compared to earlier optical poling experiments reported in **Paper I** and **Paper II**.

The poled fiber was explored in three electro-optic applications: **Paper III**, **Paper IV**, and **Paper VI**. The first explores distributed electric field sensing, the second uses intermodal interference measurements, and the last uses FBG inscribed in poled fiber. The papers show different use cases of the poled fiber devices and possible applications in electric field sensing. **Paper IV** in particular, explores the use of poled fibers with different propagating modes in the fiber, which can enable experiments in few-mode fiber sensing, few-mode modulation, and telecommunication.

The fabricated poled devices are low-loss and can easily be incorporated with standard telecom equipment, making them easy to adapt in fiber-based experiments.

References

[1] R. A. Myers, N. Mukherjee, and S. R. J. Brueck, "Large second-order nonlinearity in poled fused silica," *Opt. Lett.*, vol. 16, pp. 1732–1734, Nov 1991.

[2] P. G. Kazansky, L. Dong, and P. S. J. Russell, "High second-order nonlinearities in poled silicate fibers," *Opt. Lett.*, vol. 19, pp. 701–703, May 1994.

[3] X.-C. Long, R. Myers, and S. Brueck, "Measurement of linear electro-optic effect in temperature/electric-field poled optical fibres," *Electronics Letters*, vol. 30, pp. 2162–2163(1), December 1994.

[4] R. Kashyap, *Fiber Bragg Gratings*. Optics and Photonics, Elsevier Science, 2009.

[5] W. Margulis, O. Tarasenko, and N. Myrén, "Who needs a cathode? creating a second-order nonlinearity by charging glass fiber with two anodes," *Opt. Express*, vol. 17, pp. 15534–15540, Aug 2009.

[6] H. An and S. Fleming, "Investigating the effectiveness of thermally poling optical fibers with various internal electrode configurations," *Opt. Express*, vol. 20, pp. 7436–7444, Mar 2012.

[7] F. D. Lucia, D. Huang, C. Corbari, N. Healy, and P. J. A. Sazio, "Optical fiber poling by induction: analysis by 2d numerical modeling," *Opt. Lett.*, vol. 41, pp. 1700–1703, Apr 2016.

[8] F. D. Lucia, D. Huang, C. Corbari, N. Healy, and P. J. A. Sazio, "Optical fiber poling by induction," *Opt. Lett.*, vol. 39, pp. 6513–6516, Nov 2014.

[9] A. W. Snyder and J. Love, *Optical Waveguide Theory*. Chapman and Hall, 1 ed., 1983.

[10] J. Toulouse, "Optical nonlinearities in fibers: review, recent examples, and systems applications," *Journal of Lightwave Technology*, vol. 23, no. 11, pp. 3625–3641, 2005.

[11] B. B. Tiwari, V. Prakash, V. Tripathi, and N. Malaviya, "Nonlinear effects in optical fiber transmission system," *IETE Technical Review*, vol. 16, no. 5-6, pp. 461–479, 1999.

[12] B. E. A. Saleh and M. C. Teich, *Fundamentals of Photonics*. John Wiley & Sons, Ltd, 1991.

[13] R. Kashyap, "Phase-matched periodic electric-field-induced second-harmonic generation in optical fibers," *J. Opt. Soc. Am. B*, vol. 6, pp. 313–328, Mar 1989.

[14] D. Wong, W. Xu, S. Fleming, M. Janos, and K.-M. Lo, "Frozen-in Electrical Field in Thermally Poled Fibers," *Optical Fiber Technology*, vol. 5, pp. 235–241, Apr. 1999.

[15] A. Krotkus and W. Margulis, "Investigations of the preparation process for efficient second-harmonic generation in optical fibers," *Applied Physics Letters*, vol. 52, no. 23, pp. 1942–1944, 1988.

[16] A. Canagasabey, C. Corbari, A. V. Gladyshev, F. Liegeois, S. Guillemet, Y. Hernandez, M. V. Yashkov, A. Kosolapov, E. M. Dianov, M. Ibsen, and P. G. Kazansky, "High-average-power second-harmonic generation from periodically poled silica fibers," *Opt. Lett.*, vol. 34, pp. 2483–2485, Aug 2009.

[17] I. S. Carvalho, O. Tarasenko, A. R. Camara, J. ao M. B. Pereira, and W. Margulis, "Pockels fibers by optical poling," in *Workshop on Specialty Optical Fibers and Their Applications*, p. WT4A.22, Optica Publishing Group, 2015.

[18] "Corning®, smf-28e+® optical fiber - datasheet." `https://www.corning.com/media/worldwide/coc/documents/Fiber/PI-1463-AEN.pdf`. Accessed: 2022-04-26.

[19] D. A. Jackson, T. G. Giallorenzi, J. P. Dakin, H. C. Lefevre, R. Ulrich, R. S. Medlock, A. J. Rogers, B. Culshaw, W. H. Glenn, A. L. Harmer, and T. N. et al., *Optical fiber sensors*. Nato Science Series E:, Applied Sciences, 132, Springer Dordrecht, 1st ed. ed., 1987.

[20] E. Udd and W. B. Spillman, *Fiber optic sensors: an introduction for engineers and scientists, Second edition*. Hoboken, N.J: John Wiley & Sons, Inc, 2nd ed. ed., 2011.

[21] T. Yoshino, K. Kurosawa, K. Itoh, and T. Ose, "Fiber-optic fabry-perot interferometer and its sensor applications," *IEEE Transactions on Microwave Theory and Techniques*, vol. 30, no. 10, pp. 1612–1621, 1982.

[22] S.-M. Tseng and C.-L. Chen, "Optical fiber fabry-perot sensors," *Appl. Opt.*, vol. 27, pp. 547–551, Feb 1988.

[23] B. D. Gupta, S. K. Srivastava, and R. Verma, *Fiber Optic Sensors Based on Plasmonics*. World Scientific, 2015.

[24] A. Othonos and K. Kalli, *Fiber Bragg Gratings: Fundamentals and Applications in Telecommunications and Sensing*. Artech House Print on Demand, 1999.

[25] R. Ryf, S. Randel, A. H. Gnauck, C. Bolle, A. Sierra, S. Mumtaz, M. Esmaeelpour, E. C. Burrows, R.-J. Essiambre, P. J. Winzer, D. W. Peckham, A. H. McCurdy, and R. Lingle, "Mode-division multiplexing over 96 km of few-mode fiber using coherent 6×6 mimo processing," *Journal of Lightwave Technology*, vol. 30, no. 4, pp. 521–531, 2012.

[26] A. Alarcón, J. Argillander, G. Lima, and G. Xavier, "Few-mode-fiber technology fine-tunes losses in quantum communication systems," *Phys. Rev. Applied*, vol. 16, p. 034018, Sep 2021.

[27] F. Wang, J. Yang, L. Chen, X. Jiang, and M. Wang, "Optical switch based on multimode interference coupler," *IEEE Photonics Technology Letters*, vol. 18, no. 2, pp. 421–423, 2006.

[28] I. Ashry, Y. Mao, A. Trichili, B. Wang, T. K. Ng, M.-S. Alouini, and B. S. Ooi, "A review of using few-mode fibers for optical sensing," *IEEE Access*, vol. 8, pp. 179592–179605, 2020.

[29] T. Eftimov and W. Bock, "Sensing with a $LP_{01} - LP_{02}$ intermodal interferometer," *Journal of Lightwave Technology*, vol. 11, no. 12, pp. 2150–2156, 1993.

[30] K.-i. Kitayama and N.-P. Diamantopoulos, "Few-mode optical fibers: Original motivation and recent progress," *IEEE Communications Magazine*, vol. 55, no. 8, pp. 163–169, 2017.

[31] L. Grüner-Nielsen, N. M. Mathew, and K. Rottwitt, "Invited paper: Characterization of few mode fibers and devices," *Optical Fiber Technology*, vol. 52, p. 101972, 2019.

[32] P. Lu, N. Lalam, M. Badar, B. Liu, B. T. Chorpening, M. P. Buric, and P. R. Ohodnicki, "Distributed optical fiber sensing: Review and perspective," *Applied Physics Reviews*, vol. 6, no. 4, p. 041302, 2019.

[33] Y. R. Shen and N. Bloembergen, "Theory of stimulated brillouin and raman scattering," *Phys. Rev.*, vol. 137, pp. A1787–A1805, Mar 1965.

[34] "THORLABS - EO-PC-850 - pockels cell, 700 - 1000 nm." `https://www.thorlabs.com/thorproduct.cfm?partnumber=EO-PC-850`. Accessed: 2022-04-13.

[35] "THORLABS - LNLVL-IM-Z - low v_π intensity modulator, Z-cut, FC/PC connectors, operational up to 40 ghz, 1525 nm - 1605 nm." `https://www.thorlabs.com/thorproduct.cfm?partnumber=LNLVL-IM-Z`. Accessed: 2022-04-13.

[36] A. C. Liu, M. J. F. Digonnet, and G. S. Kino, "Measurement of the dc kerr and electrostrictive phase modulation in silica," *J. Opt. Soc. Am. B*, vol. 18, pp. 187–194, Feb 2001.

[37] G. Nadjakov, "Sur une nouvelle espece de polarisation permanente des dielectriques," *Comptes rendus de l'Académie des Sciences*, vol. 204, pp. 1865–1866, 1937.

[38] G. Nadjakov, "Uber eine neue art von elektreten: photoelektreten," *Physikalische Zeitschrift*, vol. 39, pp. 226–227, 1938.

[39] C. Marckmann, Y. Ren, G. Genty, and M. Kristensen, "Strength and symmetry of the third-order nonlinearity during poling of glass waveguides," *IEEE Photonics Technology Letters*, vol. 14, no. 9, pp. 1294–1296, 2002.

[40] J. M. Dell, M. J. Joyce, and G. O. Stone, "Erasure of poling-induced second-order optical nonlinearities in silica by UV exposure," in *Doped Fiber Devices and Systems* (M. J. F. Digonnet, ed.), vol. 2289, pp. 185 – 193, International Society for Optics and Photonics, SPIE, 1994.

[41] R. Kashyap, G. J. Veldhuis, D. C. Rogers, and P. F. Mckee, "Phase-matched second-harmonic generation by periodic poling of fused silica," *Applied Physics Letters*, vol. 64, no. 11, pp. 1332–1334, 1994.

[42] M. Fejer, G. Magel, D. Jundt, and R. Byer, "Quasi-phase-matched second harmonic generation: tuning and tolerances," *IEEE Journal of Quantum Electronics*, vol. 28, no. 11, pp. 2631–2654, 1992.

[43] T. G. Alley, S. R. J. Brueck, and M. Wiedenbeck, "Secondary ion mass spectrometry study of space-charge formation in thermally poled fused silica," *Journal of Applied Physics*, vol. 86, no. 12, pp. 6634–6640, 1999.

[44] Y. Quiquempois, N. Godbout, and S. Lacroix, "Model of charge migration during thermal poling in silica glasses: Evidence of a voltage threshold for the onset of a second-order nonlinearity," *Phys. Rev. A*, vol. 65, p. 043816, Apr 2002.

[45] N. Myrén and W. Margulis, "Time evolution of frozen-in field during poling of fiber with alloy electrodes," *Opt. Express*, vol. 13, pp. 3438–3444, May 2005.

[46] A. Camara, O. Tarasenko, and W. Margulis, "Study of thermally poled fibers with a two-dimensional model," *Opt. Express*, vol. 22, pp. 17700–17715, Jul 2014.

[47] M. Malmström, *All-fiber modulators for laser applications*. PhD thesis, KTH, 2012.

[48] R. H. Stolen and H. W. K. Tom, "Self-organized phase-matched harmonic generation in optical fibers," *Opt. Lett.*, vol. 12, pp. 585–587, Aug 1987.

[49] U. Österberg and W. Margulis, "Experimental studies on efficient frequency doubling in glass optical fibers," *Opt. Lett.*, vol. 12, pp. 57–59, Jan 1987.

[50] I. Carvalho, W. Margulis, and B. Lesche, "Preparation of frequency-doubling fibers under uv excitation," *Opt. Lett.*, vol. 16, pp. 1487–1489, Oct 1991.

[51] I. Carvalho, W. Margulis, and B. Lesche, "Erasure of frequency doubling gratings in optical fibres by ultraviolet light excitation," *Electronics Letters*, vol. 27, pp. 1497–1498(1), August 1991.

[52] T. E. Tsai, M. A. Saifi, E. J. Friebele, D. L. Griscom, and U. Österberg, "Correlation of defect centers with second-harmonic generation in ge-doped and ge–p-doped silica-core single-mode fibers," *Opt. Lett.*, vol. 14, pp. 1023–1025, Sep 1989.

[53] A. Anedda, C. Carbonaro, R. Corpino, and A. Serpi, "Absorption spectrum of ge-doped silica samples and fiber preforms in the vacuum ultraviolet region," *Journal of Non-Crystalline Solids*, vol. 280, no. 1, pp. 281–286, 2001. 3rd Symp. on SiO2 and Advanced Dielectrics.

[54] V. Nathan, A. H. Guenther, and S. S. Mitra, "Review of multiphoton absorption in crystalline solids," *J. Opt. Soc. Am. B*, vol. 2, pp. 294–316, Feb 1985.

[55] J. Du, L. René Corrales, K. Tsemekhman, and E. J. Bylaska, "Electron, hole and exciton self-trapping in germanium doped silica glass from dft calculations with self-interaction correction," *Nuclear Instruments and Methods in Physics Research Section B: Beam Interactions with Materials and Atoms*, vol. 255, no. 1, pp. 188–194, 2007. Computer Simulation of Radiation Effects in Solids.

[56] A. Alessi, S. Girard, M. Cannas, S. Agnello, A. Boukenter, and Y. Ouerdane, "Evolution of photo-induced defects in ge-doped fiber/preform: influence of the drawing," *Opt. Express*, vol. 19, pp. 11680–11690, Jun 2011.

[57] Y. Quiquempois, G. Martinelli, P. Bernage, M. Douay, P. Niay, E. Delevaque, H. Poignant, B. Loisel, and J. Bayon, "Study of organized $\Xi(2)$ susceptibility in germanosilicate optical fibers," *Optical Materials*, vol. 9, no. 1, pp. 361–367, 1998. Materials, Physics and Devices For Molecular Electronics and Photonics.

[58] T. Fujiwara, D. Wong, Y. Zhao, S. Fleming, S. Poole, and M. Sceats, "Electro-optic modulation in germanosilicate fibre with UV-excited poling," *Electronics Letters*, vol. 31, pp. 573–575, Mar. 1995.

[59] Y. Quiquempois, G. Martinelli, P. Niay, P. Bernage, M. Douay, J. F. Bayon, and H. Poignant, "Photoinscription of bragg gratings within a germanosilicate fiber subjected to a high static electric field," *Opt. Lett.*, vol. 24, pp. 139–141, Feb 1999.

[60] L. Li, R. D. Birch, and D. N. Payne, "An all-fibre electro-optic kerr modulator," in *IEE Colloquium Advanced Fibre Waveguide Devices (19/05/86)*, May 1986. Digest No. 1986/79.

[61] "Bismuth tin alloy." `https://www.americanelements.com/bismuth-tin-alloy-12010-55-8`. Accessed: 2022-04-20.

[62] F. W. Grover, *Inductance calculations: Working Formulas and Tables*. Dover Publications, Inc., special edition for instrument society of america ed., 1982.

[63] D. Lide, *CRC Handbook of Chemistry and Physics, 95th Edition*. Taylor & Francis, 2014.

[64] J. D. Jackson, *Classical electrodynamics*. Wiley, 3rd ed. ed., 1999.

[65] A. J. Ikushima, T. Fujiwara, and K. Saito, "Silica glass: A material for photonics," *Journal of Applied Physics*, vol. 88, no. 3, pp. 1201–1213, 2000.

[66] T. Erdogan, V. Mizrahi, P. J. Lemaire, and D. Monroe, "Decay of ultraviolet-induced fiber bragg gratings," *Journal of Applied Physics*, vol. 76, no. 1, pp. 73–80, 1994.

[67] P. M. P. Gouvêa and W. Margulis, "Annealing experiments in frequency-doubling fibers," *J. Opt. Soc. Am. B*, vol. 11, pp. 1515–1518, Aug 1994.

[68] D. W. Wong, W. Xu, S. C. Fleming, R. S. Hall, and M. Janos, "Recent results with thermal poling of fiber," in *Doped Fiber Devices II* (M. J. F. Digonnet and F. Ouellette, eds.), vol. 3542, pp. 120 – 123, International Society for Optics and Photonics, SPIE, 1998.

[69] X.-C. Long, R. Myers, and S. Brueck, "A poled electrooptic fiber," *IEEE Photonics Technology Letters*, vol. 8, no. 2, pp. 227–229, 1996.

[70] Y. Ren, C. Marckmann, J. Arentoft, and M. Kristensen, "Thermally poled channel waveguides with polarization-independent electrooptic effect," *IEEE Photonics Technology Letters*, vol. 14, no. 5, pp. 639–641, 2002.

[71] N. Godbout, S. Lacroix, Y. Quiquempois, G. Martinelli, and P. Bernage, "Measurement and calculation of electrostrictive effects in a twin-hole silica glass fiber," *J. Opt. Soc. Am. B*, vol. 17, pp. 1–5, Jan 2000.

[72] O. Tarasenko, N. Myren, W. Margulis, and I. Carvalho, "All-fiber electrooptical polarization control," in *2006 Optical Fiber Communication Conference and the National Fiber Optic Engineers Conference*, p. 3, 2006.

[73] J. M. B. Pereira, J. Hervás, D. Barrera, J. Madrigal, S. Sales, F. Laurell, O. Tarasenko, and W. Margulis, "High-voltage fiber sensor based on fiber Bragg grating in poled fiber," in *Seventh European Workshop on Optical Fibre Sensors* (K. Kalli, S. O. O'Keeffe, and G. Brambilla, eds.), vol. 11199, pp. 467 – 470, International Society for Optics and Photonics, SPIE, 2019.

[74] Z. Yu, P.-Y. Fonjallaz, W. Margulis, and O. Tarasenko, "High-speed switching of a DFB grating in a twin-hole fibre," in *Passive Components and Fiber-based Devices V* (M.-J. Li, P. Shum, I. H. White, and X. Wu, eds.), vol. 7134, pp. 425 – 432, International Society for Optics and Photonics, SPIE, 2008.

[75] W. Margulis, F. Laurell, and B. Lesche, "Imaging the nonlinear grating in frequency-doubling fibres," *Nature*, vol. 378, pp. 699–701, Dec 1995.

[76] O. Tarasenko and W. Margulis, "The effect of the electrode curvature on the field in internal electrode fibers," *IEEE Photonics Technology Letters*, vol. 27, no. 20, pp. 2131–2133, 2015.

[77] M.-V. Bergot, M. C. Farries, M. E. Fermann, L. Li, L. J. Poyntz-Wright, P. S. J. Russell, and A. Smithson, "Generation of permanent optically induced second-order nonlinearities in optical fibers by poling," *Opt. Lett.*, vol. 13, pp. 592–594, Jul 1988.

[78] V. Mizrahi and J. E. Sipe, "Generation of permanent optically induced second-order nonlinearities in optical fibers by poling: comment," *Appl. Opt.*, vol. 28, pp. 1976–1976, Jun 1989.

[79] P. G. Kazansky, L. Dong, P. Hua, and P. S. J. Russell, "High second-order nonlinearities in poled silica fibers," in *Conference on Lasers and Electro-Optics*, p. CFC3, Optica Publishing Group, 1994.

[80] "Osram hns 55 w g13." `https://www.osram.com/ecat/PURITEC%20HNS%20UV-C-UV-C%20lamps%20for%20purification-Ultraviolet%20lamps-Industry-Specialty%20Lighting/com/en/GPS01_1028570/ZMP_4021031/`. accessed: 2022-04-28.

[81] J. Pastor-Graells, H. F. Martins, A. Garcia-Ruiz, S. Martin-Lopez, and M. Gonzalez-Herraez, "Single-shot distributed temperature and strain tracking using direct detection phase-sensitive otdr with chirped pulses," *Opt. Express*, vol. 24, pp. 13121–13133, Jun 2016.

[82] M. R. Fernández-Ruiz, L. Costa, and H. F. Martins, "Distributed acoustic sensing using chirped-pulse phase-sensitive otdr technology," *Sensors*, vol. 19, no. 20, 2019.

[83] T. A. Birks, I. Gris-Sánchez, S. Yerolatsitis, S. G. Leon-Saval, and R. R. Thomson, "The photonic lantern," *Adv. Opt. Photon.*, vol. 7, pp. 107–167, Jun 2015.

Appendix A

Electric field interaction in an optical media

The polarization of the light P in an optical media is affected by the electric field E with the expression [12]:

$$P(E) = \epsilon_0 \left(\chi E + \chi^{(2)} E^2 + \chi^{(3)} E^3 \right) \tag{A.1}$$

where ϵ_0 is the permittivity in free space, χ is the linear susceptibility, $\chi^{(2)}$ and $\chi^{(3)}$ are the second-order and third-order nonlinear coefficients. Higher order terms are neglected. A linear media is characterized with a linear dependence of the polarization with the field and only the first term is used, $P(E) = \epsilon_0 \chi E$. χ is related to the dielectric constant of the material and the refractive index with $n^2 = \epsilon/\epsilon_0 = 1 + \chi$.

The electric field from an optical wave with frequency ω and amplitude $E(\omega)$ can be written as

$$E'(t) = Re\{E(\omega) exp(j\omega t)\} \tag{A.2}$$

In a second order nonlinear media, the nonlinear component of the polarization is

$$P_{NL} = \epsilon_0 \chi^{(2)} E^2 \tag{A.3}$$

Substituting A.2 in A.3 gives the nonlinear term of the polarization, $P_{NL}(t)$ [12]:

$$P_{NL}(t) = P_{NL}(0) + (Re\{P_{NL}(2\omega) exp(j2\omega t)\}) \tag{A.4}$$

where

$$P_{NL}(0) = \epsilon_0 \chi^{(2)} E(\omega) E^*(\omega) \tag{A.5}$$

$$P_{NL}(2\omega) = \epsilon_0 \chi^{(2)} E(\omega) E(\omega) \tag{A.6}$$

From here it is noted that a second-order nonlinear media generates an electromagnetic radiation with doubled the frequency (2ω) of the excited radiation (ω).

If the electric field is a sum of a steady component ($\omega = 0$) applied externally and the optical field, the equation A.2 can be rewritten as:

$$E'(t) = E(0) + Re\{E(\omega) exp(j\omega t)\} \tag{A.7}$$

Substituting A.7 in A.3 for a second order nonlinear media gives [12]:

$$P_{NL}(t) = P_{NL}(0) + Re\{P_{NL}(\omega) exp(j\omega t)\} + Re\{P_{NL}(2\omega) exp(j2\omega t)\} \tag{A.8}$$

where

$$P_{NL}(0) = \epsilon_0 \chi^{(2)} E(\omega) E^*(\omega) \tag{A.9}$$

$$P_{NL}(\omega) = \epsilon_0 \chi^{(2)} E(\omega) E(\omega) \tag{A.10}$$

$$P_{NL}(2\omega) = \epsilon_0 \chi^{(2)} E(\omega) E(\omega) \tag{A.11}$$

Appendix B

Paper Reprints